mTORC1 and mTORC2 selectively regulate CD8$^+$ T cell differentiation

Kristen N. Pollizzi,[1] Chirag H. Patel,[1] Im-Hong Sun,[1] Min-Hee Oh,[1] Adam T. Waickman,[1,2] Jiayu Wen,[1] Greg M. Delgoffe,[1,3] and Jonathan D. Powell[1]

[1]Sidney-Kimmel Comprehensive Cancer Research Center, Department of Oncology, Johns Hopkins University School of Medicine, Baltimore, Maryland, USA. [2]Experimental Immunology Branch, National Cancer Institute, NIH, Bethesda, Maryland, USA. [3]Department of Immunology, University of Pittsburgh, Pittsburgh, Pennsylvania, USA.

Activation of mTOR-dependent pathways regulates the specification and differentiation of CD4$^+$ T effector cell subsets. Herein, we show that mTOR complex 1 (mTORC1) and mTORC2 have distinct roles in the generation of CD8$^+$ T cell effector and memory populations. Evaluation of mice with a T cell–specific deletion of the gene encoding the negative regulator of mTORC1, tuberous sclerosis complex 2 (TSC2), resulted in the generation of highly glycolytic and potent effector CD8$^+$ T cells; however, due to constitutive mTORC1 activation, these cells retained a terminally differentiated effector phenotype and were incapable of transitioning into a memory state. In contrast, CD8$^+$ T cells deficient in mTORC1 activity due to loss of RAS homolog enriched in brain (RHEB) failed to differentiate into effector cells but retained memory characteristics, such as surface marker expression, a lower metabolic rate, and increased longevity. However, these RHEB-deficient memory-like T cells failed to generate recall responses as the result of metabolic defects. While mTORC1 influenced CD8$^+$ T cell effector responses, mTORC2 activity regulated CD8$^+$ T cell memory. mTORC2 inhibition resulted in metabolic reprogramming, which enhanced the generation of CD8$^+$ memory cells. Overall, these results define specific roles for mTORC1 and mTORC2 that link metabolism and CD8$^+$ T cell effector and memory generation and suggest that these functions have the potential to be targeted for enhancing vaccine efficacy and antitumor immunity.

Introduction

CD8$^+$ T cells are an essential component of the adaptive immune response, generating both effector cells necessary for clearance of acute infection and long-lived memory cells primed to provide a rapid secondary response (1). Upon initial encounter with antigen, naive CD8$^+$ T cells rapidly proliferate to generate effector cells (2). Such cells have enormous metabolic demands and rely in part on aerobic glycolysis as a means of promoting effector activation (3, 4). In contrast, CD8$^+$ memory T cells, which are programmed for long-term survival, have fewer acute metabolic needs and use oxidative phosphorylation rather than glycolysis (5, 6). While recent work has indicated the importance of metabolic programming in T cell fate, the pathways that regulate T cell metabolism are still being elucidated (7).

mTOR is an evolutionarily conserved serine/threonine protein kinase important for the integration of environmental cues to regulate cellular metabolism, protein synthesis, differentiation, survival, and growth (8). mTOR exists as two distinct protein complexes, mTOR complex 1 (mTORC1) and mTORC2, each with unique functions and downstream targets. The activation of mTORC1 has been well characterized. Negative regulators of mTORC1, tuberous sclerosis complex 1 (TSC1), TSC2, and newly described TBC1D7 (9), form a protein complex functioning as a GAP for RAS homolog enriched in brain (RHEB) (10, 11). Upon inhibitory phosphorylation of TSC1 or TSC2, the TSC1/2 complex disassociates, allowing for accumulation of RHEB-GTP. RHEB-GTP interacts with mTORC1, leading to mTOR kinase activity, measured as an increase in the phosphorylation of the mTORC1 substrates S6K-1 and 4E-BP1 (12). Several studies have examined the role of TSC1 in T cells and have demonstrated its critical role in promoting survival (13–16). The role of TSC2 in T cells has yet to be determined.

In CD4$^+$ T cells, mTORC1 and mTORC2 have emerged as critical integrators of signals from the immune microenvironment. mTORC1 selectively regulates Th1 and Th17 differentiation, while mTORC2 promotes the generation of Th2 cells (17, 18). Furthermore, complete inhibition of mTOR activity in CD4$^+$ T cells results in the generation of regulatory T cells, even under normally activating conditions (19). Therefore, we were interested in determining the specific roles of mTORC1 and mTORC2 signaling in regulating CD8$^+$ T cell effector and memory generation. In this report, we demonstrate a critical role for mTORC1 and mTORC2 in regulating CD8$^+$ T cell effector and memory differentiation.

Results

TSC2 integrates signals to regulate CD8$^+$ effector function. TSC2 negatively regulates mTORC1 activity by acting as a GAP for the mTORC1-activitating GTPase RHEB (20). Upon phosphorylation by AKT or ERK, TSC2 is inactivated, thus leading to increased mTORC1 activity (8). In order to dissect how mTORC1 integrates signals in CD8$^+$ T cells, we created mice in which TSC2 is selectively deleted in T cells (*Cd4-Cre Tsc2$^{fl/fl}$* mice, herein referred to as T-*Tsc2$^{-/-}$* mice) (Supplemental Figure 1A; supplemental material available online with this article; doi:10.1172/JCI77746DS1).

Conflict of interest: The authors have declared that no conflict of interest exists.
Submitted: July 1, 2014; **Accepted:** March 12, 2015.
Reference information: *J Clin Invest*. 2015;125(5):2090–2108. doi:10.1172/JCI77746.

Consistent with its role in negatively regulating mTORC1 activity, *Tsc2* deletion in CD8$^+$ T cells resulted in elevated phosphorylation of ribosomal S6 kinase 1 (S6K1), ribosomal S6, and 4E-BP1 under both unstimulated and TCR-stimulated conditions (Figure 1A and Supplemental Figure 1B) (21). mTORC2 activity, as assessed by phosphorylation of AKT at S473, was still intact in T-*Tsc2*$^{-/-}$ CD8$^+$ T cells following TCR stimulation, albeit slightly reduced from WT levels (Figure 1A). Phenotypic analysis of T-*Tsc2*$^{-/-}$ mice revealed normal percentages and absolute numbers of T and B cells but a decreased CD8$^+$ to CD4$^+$ T cell ratio (Figure 1B and Supplemental Figure 1, C–E). As TSC2 is deleted after the double-positive stage of thymic development, we suspect that these altered CD4/CD8 ratios reflect post-thymic events. Further analysis revealed that T-*Tsc2*$^{-/-}$ CD8$^+$ and CD4$^+$ T cells have an increased CD44^{hi}CD62L^{lo} population, indicative of an activated phenotype (Figure 1C). Consistent with this activated phenotype, T-*Tsc2*$^{-/-}$ CD8$^+$ and CD4$^+$ T cells exhibited enhanced proliferation upon TCR engagement compared with WT cells (Figure 1D).

The role of TSC2 in T cells has yet to be described. Recent reports have examined the role of TSC1 in T cells and have observed increases in apoptosis in TSC1-deficient T cells (13–16). The increased apoptosis was associated with decreased AKT activity and decreased expression of the antiapoptotic proteins, BCL-2 and BCL-XL. In contrast, ex vivo survival and activation-induced cell death were equivalent in T-*Tsc2*$^{-/-}$ and WT CD8$^+$ T cells (Supplemental Figure 1, F and G). Unlike that observed in *Tsc1*$^{-/-}$ T cells, T-*Tsc2*$^{-/-}$ CD8$^+$ T cells had equivalent levels of BCL-2 and BCL-XL when compared with those in WT CD8$^+$ T cells (Supplemental Figure 1, H and I). Thus, while TSC1 deletion leads to increased cell death in T cells, TSC2 deletion results in enhanced proliferation and activation. Mechanistically, these differences seem to reflect the fact that the *Tsc1*$^{-/-}$ T cells lack mTORC2 activity, as indicated by impaired phosphorylation of AKT at S473 (13, 14, 16), while in T-*Tsc2*$^{-/-}$ CD8$^+$ T cells, AKT activity was relatively intact (Figure 1A). Additionally, TSC1 deficiency resulted in a loss of TSC2 protein, while TSC1 expression was intact in T-*Tsc2*$^{-/-}$ cells (Supplemental Figure 1J) (22).

Next, we wanted to determine the effect of TSC2 deficiency on the function of CD8$^+$ effector T cells. As expected, T-*Tsc2*$^{-/-}$ CD8$^+$ T cells demonstrated enhanced mTORC1 activation but intact mTORC2 signaling (Figure 2, A and B). Furthermore, upon restimulation, T-*Tsc2*$^{-/-}$ CD8$^+$ T cells exhibited enhanced production of IFN-γ and TNF-α, in addition to increased granzyme B expression (Figure 2C). This increase in IFN-γ production was detected in T-*Tsc2*$^{-/-}$ CD8$^+$ T cells by 24 hours after initial stimulation (Supplemental Figure 2A). Furthermore, an increase in IFN-γ production was also detected in T-*Tsc2*$^{-/-}$ CD4$^+$ T cells (Supplemental Figure 2B).

To determine whether the enhanced effector function observed in T-*Tsc2*$^{-/-}$ CD8$^+$ T cells was due to previous activation, we assessed cytokine production of sorted naive CD8$^+$ T cells. Stimulation of naive T-*Tsc2*$^{-/-}$ CD8$^+$ T cells resulted in elevated IFN-γ and TNF-α production, compared with that in stimulated naive WT CD8$^+$ T cells (Figure 2D), in addition to increased proliferation (Figure 2E). Thus, while T cells from T-*Tsc2*$^{-/-}$ mice have a propensity to have an activated phenotype, the enhanced effector function and proliferative capacity of T-*Tsc2*$^{-/-}$ CD8$^+$ T cells is not simply a consequence of previous activation.

As constitutive activation of mTORC1, through *Tsc2* deletion, resulted in enhanced effector generation, we also wanted to determine whether mTORC1 activity was required for the generation of CD8$^+$ effector T cells. To this end, we assessed effector function of T cells deficient in RHEB (*Cd4-Cre Rheb*$^{fl/fl}$ cells, herein referred to as T-*Rheb*$^{-/-}$ CD8$^+$ T cells) (17, 23). RHEB is a small GTPase that is negatively regulated by the GAP activity of TSC2 and plays a critical role in the immediate activation of mTORC1 (10). T-*Rheb*$^{-/-}$ CD8$^+$ T cells have reduced mTORC1 activity but intact mTORC2 signaling (Figure 2, A and B). Upon stimulation, T-*Rheb*$^{-/-}$ CD8$^+$ T cells have markedly diminished expression of IFN-γ, TNF-α, and granzyme B when compared with that of WT T cells (Figure 2C). The inability of T-*Rheb*$^{-/-}$ CD8$^+$ T cells to produce cytokines was not due to a proliferative defect, as T-*Rheb*$^{-/-}$ CD8$^+$ T cells are capable of dividing, albeit at a delayed rate compared with that of WT cells, upon stimulation (Supplemental Figure 2A). T-*Rheb*$^{-/-}$ CD8$^+$ T cells also demonstrated expression of activation markers CD69 and CD44 that was equivalent to that in WT and T-*Tsc2*$^{-/-}$ cells, suggesting that they do not have a defect in TCR stimulation (Supplemental Figure 2C). Interestingly, while T-*Rheb*$^{-/-}$ CD8$^+$ T cells express decreased levels of effector molecules, they exhibited increased expression of CD127 (IL-7Rα receptor), which is critical for CD8$^+$ memory survival (Figure 2F) (24).

Next, we moved to an in vivo model. WT, T-*Rheb*$^{-/-}$, and T-*Tsc2*$^{-/-}$ mice were infected with a recombinant vaccinia virus that expresses ovalbumin (vaccinia-OVA), and 6 days later, the generation and function of OVA-specific CD8$^+$ effector T cells was determined using OVA tetramer (H-2 kb/ SIINFEKL) staining. T-*Tsc2*$^{-/-}$ mice exhibited a robust increase in the number of activated antigen-specific CD8$^+$ T cells compared with that of WT mice (Figure 3A). OVA-specific T-*Tsc2*$^{-/-}$ CD8$^+$ T cells exhibited increased expression of KLRG1, a marker of terminally differentiated effector CD8$^+$ T cells (Figure 3B and ref. 25), and robust IFN-γ and TNF-α production (Figure 3C). Consistent with an enhanced effector phenotype, OVA-specific CD8$^+$ T cells from T-*Tsc2*$^{-/-}$ mice had markedly increased expression of T-bet, a transcription factor associated with CD8$^+$ effector phenotype (Supplemental Figure 2D and ref. 26). Furthermore, T-*Tsc2*$^{-/-}$ CD8$^+$ T cells demonstrated high cytolytic function, as determined by an in vivo cytotoxic T lymphocyte (CTL) assay (Figure 3D). In contrast, T-*Rheb*$^{-/-}$ CD8$^+$ T cells, which have reduced mTORC1 signaling, have reduced numbers of antigen-specific T cells; expressed decreased levels of KLRG1, IFN-γ, TNF-α, and T-bet; and demonstrated decreased cytolytic function (Figure 3 and Supplemental Figure 2D). However, similar to our in vitro findings, OVA-specific T-*Rheb*$^{-/-}$ CD8$^+$ T cells demonstrated elevated expression of CD127 compared with WT cells, while OVA-specific T-*Tsc2*$^{-/-}$ CD8$^+$ T cells had the lowest expression (Supplemental Figure 2E). Thus, hyperactivation of mTORC1 leads to enhanced accumulation of potent CD8$^+$ T effector cells in vivo, while mTORC1 deficiency promotes CD127 expression.

Next, we crossed all genotypes onto the OT-I background, so that the mice expressed a TCR specific for the OVA MHC class I peptide, SIINFEKL. OT-I$^+$ WT, T-*Rheb*$^{-/-}$, and T-*Tsc2*$^{-/-}$ mice all have similar development of SIINFEKL-specific CD8$^+$ T cells, with 98% of CD8$^+$ splenocytes expressing the Vβ5.1/Vβ5.2 TCR (Supplemental Figure 3A). OT-I$^+$ WT, T-*Rheb*$^{-/-}$, and T-*Tsc2*$^{-/-}$ CD8$^+$

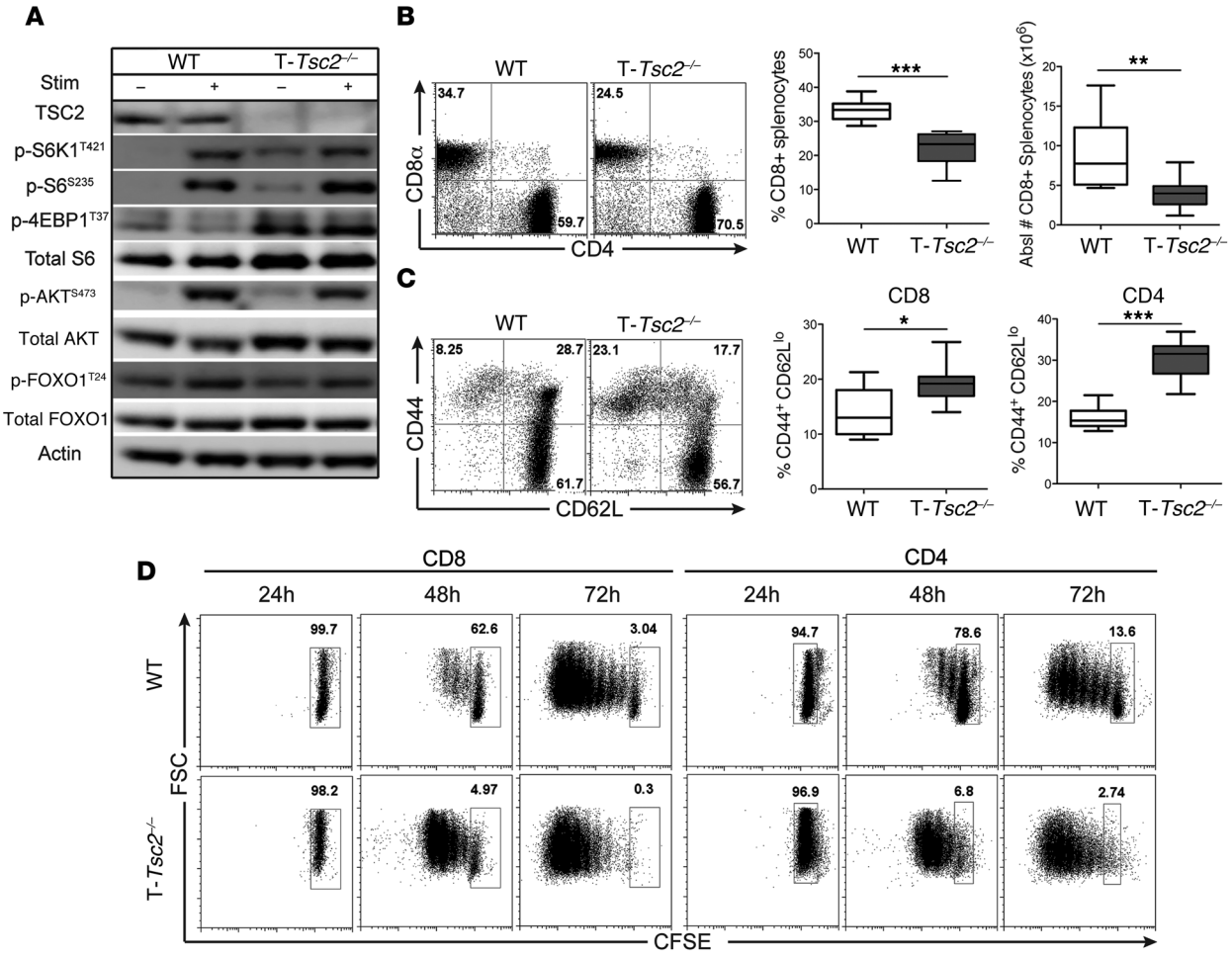

Figure 1. *Tsc2* deletion in CD8⁺ T cells yields a hyperactivated phenotype. WT and T-*Tsc2*$^{-/-}$ splenocytes were harvested from 6-week-old mice. (**A**) mTORC1 and mTORC2 activity was assessed by immunoblot analysis from isolated CD8⁺ T cells left unstimulated or after 3-hour αCD3/αCD28 stimulation. (**B**) Flow cytometric analysis of CD4 and CD8 expression gated from CD3⁺ cells and the mean percentage and absolute number of CD8⁺ T cells (n = 9). (**C**) Flow cytometric analysis of CD44 and CD62L expression gated from the CD8⁺ population, with statistics shown to the right for both CD8⁺ and CD4⁺ T cells (n = 9). (**D**) CFSE-labeled splenocytes from WT and T-*Tsc2*$^{-/-}$ mice were stimulated with αCD3. CFSE dilution of CD8⁺ and CD4⁺ T cell populations was determined following 24, 48, and 72 hours of stimulation. Data are representative of at least 3 independent experiments. For the box-and-whiskers plots, the whiskers represent the minimum and maximum values, the box boundaries represent the 25th and 75th percentiles, and the middle line is the median value. *P < 0.05, **P < 0.01, ***P < 0.001, Mann-Whitney t tests.

T cells congenically marked with CD90.1 were adoptively transferred into WT CD90.2⁺ recipients that were infected with vaccinia-OVA. Six days after infection, the percentage of OT-I⁺ splenocytes was assessed. Consistent with our endogenous findings, T-*Tsc2*$^{-/-}$ CD8⁺ T cells exhibited dramatically enhanced numbers of antigen-specific cells and increased BrdU uptake, in addition to increased KLRG1 expression and effector cytokine production (Figure 4A and Supplemental Figure 3B). In contrast, CD8⁺ T cells from T-*Rheb*$^{-/-}$ mice demonstrated markedly impaired expansion, diminished KLRG1 expression, reduced production of effector cytokines IFN-γ and TNF-α, and reduced BrdU uptake (Figure 4A and Supplemental Figure 3B). Overall, these findings demonstrate the ability of TSC2 to regulate CD8⁺ T cell effector generation through cell-intrinsic regulation of mTORC1.

As with our in vitro experiments, we repeated the adoptive transfer with a starting population of sorted naive CD8⁺ T cells. Naive T-*Tsc2*$^{-/-}$ antigen-specific CD8⁺ T cells demonstrated increased cytokine production compared with WT cells after vaccinia-OVA infection (Supplemental Figure 3C). Interestingly, the adoptive transfer of naive T-*Tsc2*$^{-/-}$ OT-I⁺ T cells did not consistently display a proliferative advantage when compared with WT T cells (Supplemental Figure 3C). This is in contrast to our finding that naive T-*Tsc2*$^{-/-}$ CD8⁺ T cells proliferate to a greater extent than naive WT T cells after in vitro stimulation (Figure 2E). Thus, for unclear reasons, while in vivo endogenous and adoptively transferred T-*Tsc2*$^{-/-}$ CD8⁺ T cells (Figure 3A and Figure 4A) and in vitro naive T-*Tsc2*$^{-/-}$ CD8⁺ T cells (Figure 2E) proliferated to a greater extent than WT T cells, adoptively transferred naive OT-I⁺ T-*Tsc2*$^{-/-}$ CD8⁺ T cells did not.

Next, we wanted to determine the ability of such cells to reject tumors. To this end, T-*Tsc2*$^{-/-}$ and WT mice were challenged with a s.q. injection of an EL4 thymoma line engineered to express luciferase. T-*Tsc2*$^{-/-}$ mice cleared the tumor, while the tumors in WT mice had an exponential increase in growth, as

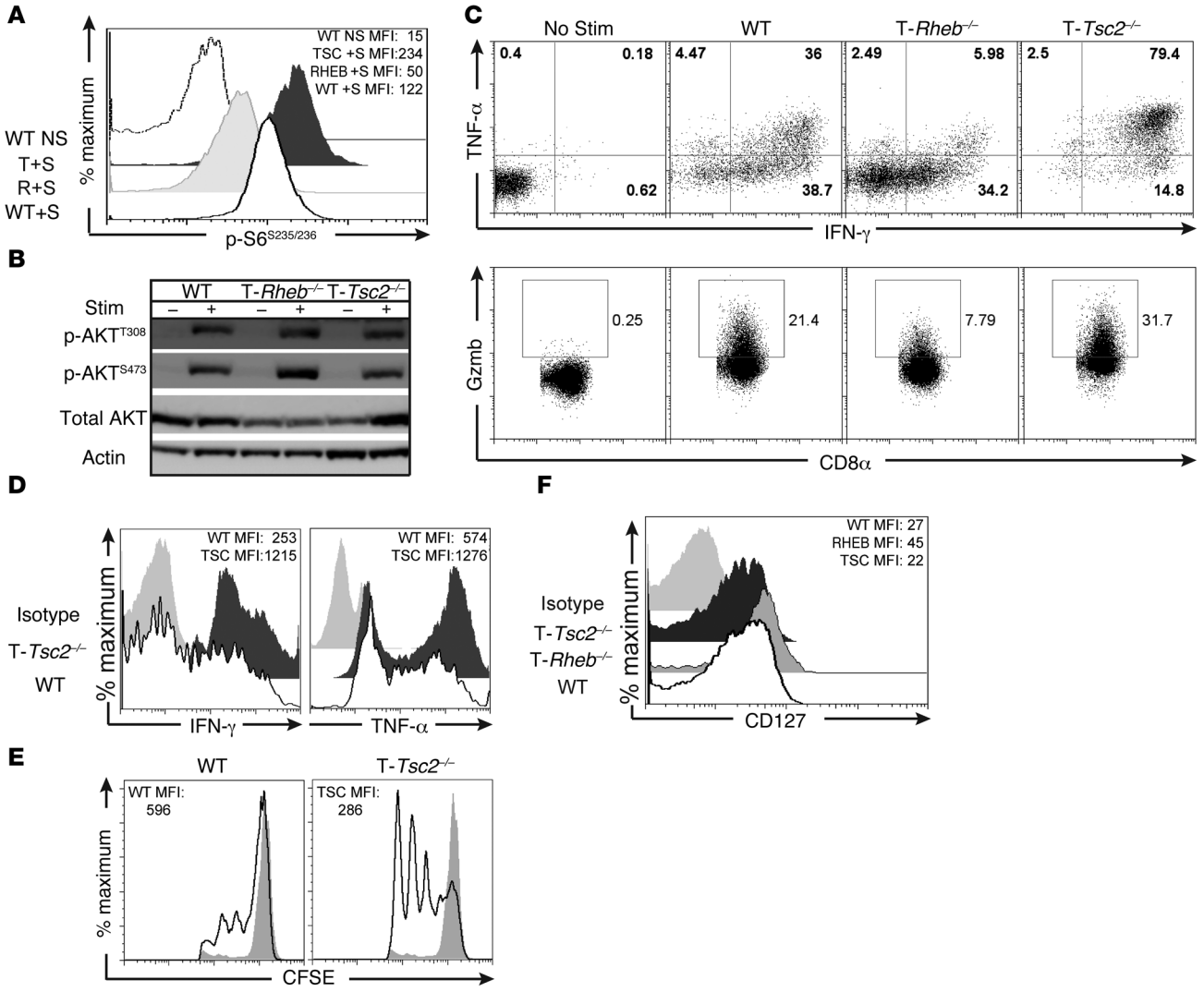

Figure 2. mTORC1 activity is required to promote CD8⁺ effector T cell responses in vitro. (**A**) mTORC1 activity was assessed by flow cytometric analysis of phosphorylated $S6^{S235/236}$ expression from WT, T-*Tsc2*$^{-/-}$, and T-*Rheb*$^{-/-}$ purified CD8⁺ T cells stimulated (+S) for 48 hours with αCD3/αCD28 compared with unstimulated WT controls (WT NS). The mean fluorescence intensity (MFI) for each genotype is shown in the upper corner. (**B**) Purified CD8⁺ T cells were collected from WT, T-*Rheb*$^{-/-}$, or T-*Tsc2*$^{-/-}$ mice. mTORC2 activity was assessed by immunoblot analysis from unstimulated cells or after 1.5-hour stimulation with αCD3/αCD28. (**C**) Splenocytes were stimulated in vitro with αCD3 for 48 hours and then expanded in media supplemented with IL-2 for 5 days. On day 5, cells were restimulated and intracellular production of IFN-γ, TNF-α, and granzyme B (GzmB) was measured by flow cytometry. Plots are gated from the CD8⁺ population. (**D**) Cytokine production and (**E**) CFSE dilution were determined from purified naive CD8⁺ WT and T-*Tsc2*$^{-/-}$ CD8⁺ T cells stimulated in vitro. Plots were gated from the CD8⁺ population. CFSE expression was measured 48 hours after stimulation. Nonstimulated controls shown as gray histograms. (**F**) As in **C**, CD127 expression of the CD8⁺ population was assessed by flow cytometry prior to restimulation. Data are representative of at least 3 independent experiments.

indicated by luciferase signal (Figure 4B). Furthermore, when challenged with EL-4 tumor cells, 100% of the T-*Tsc2*$^{-/-}$ mice survived past day 40, while WT mice did not (Supplemental Figure 7F). The enhanced ability of T-*Tsc2*$^{-/-}$ CD8⁺ T cells to reject tumor was recapitulated in a B16 melanoma model. Adoptive transfer of in vitro–activated T-*Tsc2*$^{-/-}$ OT-I⁺ T cells into WT mice challenged with OVA-expressing B16 melanoma tumor cells resulted in slower tumor growth and a greater survival advantage than transfer of littermate control (*Tsc2*$^{fl/fl}$ or *Rheb*$^{fl/fl}$) OT-I⁺ T cells (Figure 4, C–E, and Supplemental Figure 4A). In contrast, transfer of activated T-*Rheb*$^{-/-}$ OT-I⁺ cells offered the least protection (Figure 4, C–E). Tumor growth in Figure 4C is statistically significant, based on repeated-measures analysis with respect to group and time (see *Statistics*). Furthermore, T-*Rheb*$^{-/-}$ mice developed the greatest tumor burden compared with that of littermate controls in an EL4 tumor model (Supplemental Figure 4B).

Constitutive activation of mTORC1 yields terminally differentiated effector cells at the expense of memory formation. Although T-*Tsc2*$^{-/-}$ cells do not have a survival defect prior to or after acute stimulation, 6 days after vaccinia-OVA infection, OVA-specific T-*Tsc2*$^{-/-}$ CD8⁺ T cells have enhanced expression of active caspase-3 and low expression of BCL-2, while OVA-specific T-*Rheb*$^{-/-}$ CD8⁺ T cells have the highest BCL-2 expression (Supplemental

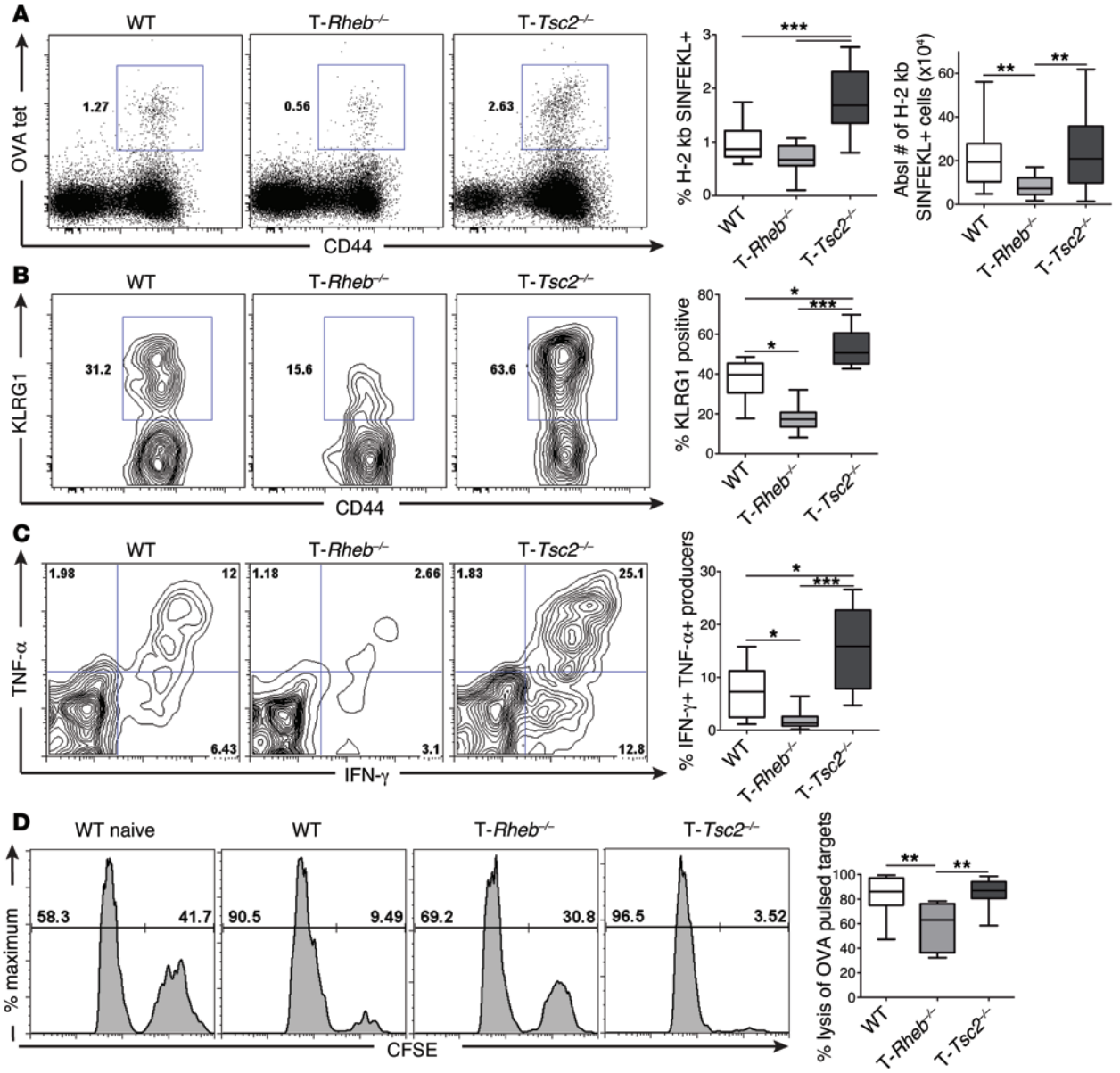

Figure 3. mTORC1 activity is required for effector generation in vivo. WT, T-*Rheb*$^{-/-}$, and T-*Tsc2*$^{-/-}$ mice were infected with 1×10^6 PFU vaccinia-OVA. On day 6, splenocytes were harvested. (**A**) Percentage of antigen-specific CD8$^+$ T cells from day 6 infected mice was determined by flow cytometric analysis of H-2 kb/SIINFEKL tetramer staining (OVA tet). Plots were gated from the CD8$^+$ population. Graphs depict the percentage of tetramer$^+$ cells from the CD8$^+$ population and the absolute number of tetramer$^+$ cells (n = 16). (**B**) KLRG1 expression was assessed from the tetramer$^+$ population, with statistics shown to the right (n = 16). (**C**) Cytokine production was assessed from the CD44$^+$CD8$^+$ splenic populations after ex vivo stimulation with SIINFEKL peptide. The graph depicts the percentage of double-producing cells (n = 16). (**D**) Functional analysis of CD8$^+$ T cells by an in vivo CTL assay 6 days after vaccinia-OVA infection. Plots depict CFSE^{hi} SIINFEKL peptide–pulsed targets and CFSE^{lo} control targets recovered from splenocytes harvested 10 hours after target transfer, with statistics shown to the right (n = 18). Data are representative of at least 3 independent experiments. For the box-and-whiskers plots, the whiskers represent the minimum and maximum values, the box boundaries represent the 25th and 75th percentiles, and the middle line is the median value. *P < 0.05, **P < 0.01, ***P < 0.001, ANOVA.

Figure 5, A and B). Thus, we wanted to determine the potential role of TSC2 and RHEB in regulating T cell memory. WT, T-*Rheb*$^{-/-}$, and T-*Tsc2*$^{-/-}$ mice were infected with vaccinia-OVA and tetramer-positive T cells were assessed 30 days following infection. In contrast to our findings during acute infection, 30 days after infection we observed a 2-fold increase of activated, antigen-specific CD8$^+$ T cells in T-*Rheb*$^{-/-}$ mice compared with that in WT mice (Figure 5A and Supplemental Figure 5C). This result is consistent with previous studies demonstrating that rapamycin can promote the generation of memory cells (27, 28). There was a 2-fold reduction of antigen-specific cells in T-*Tsc2*$^{-/-}$ mice compared with that in WT mice (Figure 5A and Supplemental Figure 5C). Importantly, T-*Rheb*$^{-/-}$ T cells failed to respond to SIINFEKL upon rechallenge (Figure 5, B and C). Alternatively, the few T-*Tsc2*$^{-/-}$ CD8$^+$ T cells that still remained at this late time point responded robustly. Thus, these data indicate that, while RHEB deficiency results in

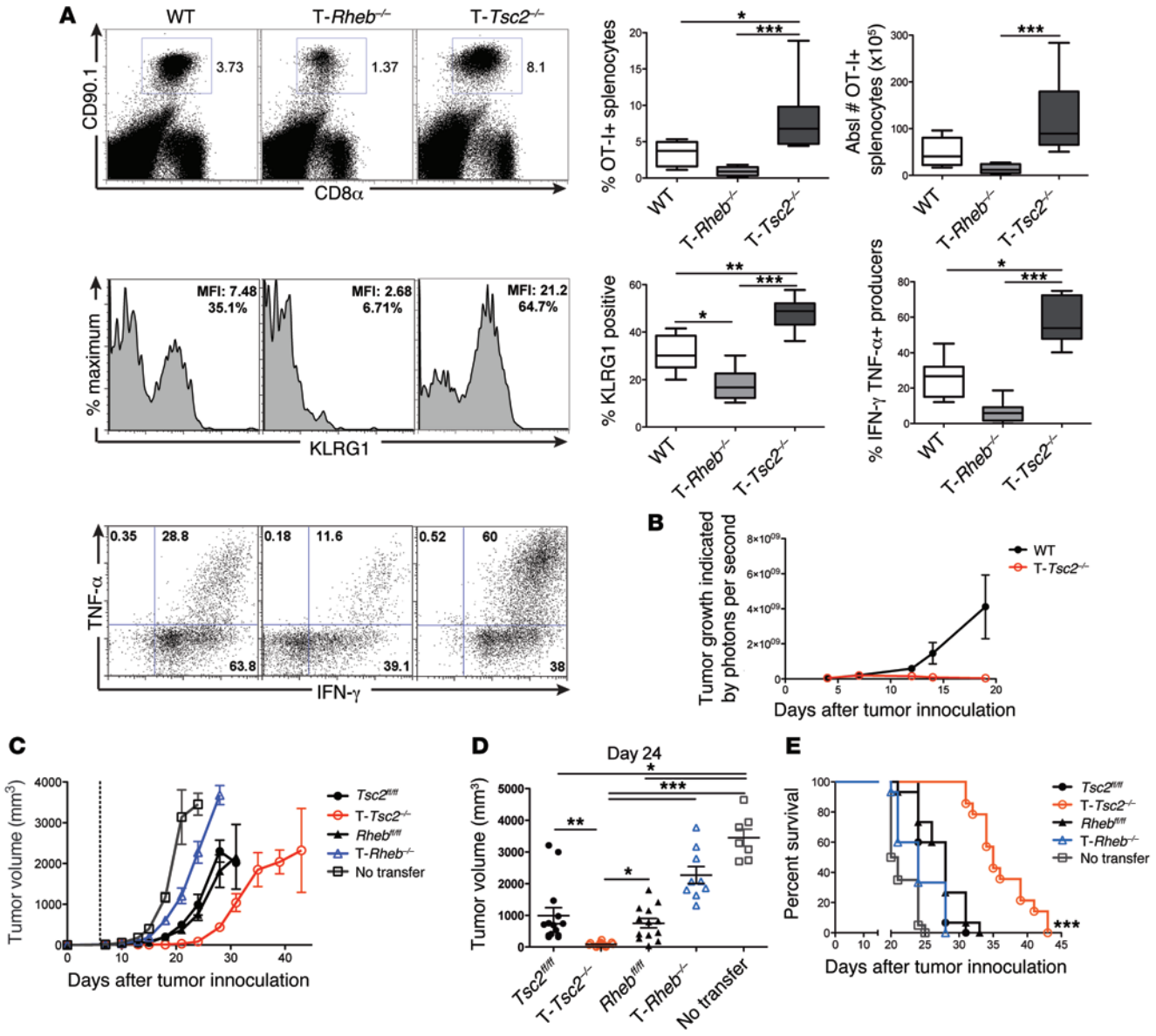

Figure 4. The ability of hyperactive mTORC1 signaling to promote effector function is cell intrinsic. (**A**) OT-I$^+$CD90.1$^+$CD8$^+$ T cells from WT, T-*Rheb*$^{-/-}$, and T-*Tsc2*$^{-/-}$ mice were adoptively transferred into WT CD90.2$^+$ recipient mice infected with vaccinia-OVA. Six days after infection, splenocytes were harvested. The percentage of splenic CD8$^+$ CD90.1$^+$ T cells, KLRG1 expression of CD8$^+$CD90.1$^+$ cells, and IFN-γ and TNF-α production after SIINFEKL peptide stimulation are shown, with statistics to the right (n = 10). For the box-and-whiskers plots, the whiskers represent the minimum and maximum values, the box boundaries represent the 25th and 75th percentiles, and the middle line is the median value. (**B**) WT and T-*Tsc2*$^{-/-}$ mice received s.q. EL4 thymoma cells expressing luciferase. Tumor burden was assessed by detection of luminescence (n = 16). (**C**–**E**) In vitro–activated T-*Rheb*$^{-/-}$ and T-*Tsc2*$^{-/-}$ and littermate control OT-I$^+$CD8$^+$ T cells were injected into WT recipients that had received B16-OVA cells 6 days prior (dashed line represents T cell transfer). "No transfer" indicates that mice did not receive OT-I$^+$ cells. (**C**) Tumor volume was assessed every 2 to 3 days. Each symbol represents an average per genotype (n = 15). (**D**) Tumor volume shown at day 24 after tumor inoculation. Each dot represents a mouse. Data are derived from **C**. (**E**) Survival was assessed. Mice that received T-*Tsc2*$^{-/-}$ cells had enhanced survival compared with all other treatments, as determined by multiple comparisons Mantel-Cox tests. Statistics in **A** and **D** were determined by ANOVA and for **B** and **C** were determined by repeated-measures analysis. Data are representative of at least 3 independent experiments. *P < 0.05, **P < 0.01, ***P < 0.001

enhanced longevity of antigen-specific cells, these cells fail to respond upon rechallenge, suggesting that they do not possess true memory characteristics.

We hypothesized that the decrease in memory T cells observed in the T-*Tsc2*$^{-/-}$ mice was the result of persistent mTORC1 activation inhibiting the upregulation of the cellular programs necessary for long-term survival. To test this hypothesis, WT and T-*Tsc2*$^{-/-}$ OT-I$^+$ T cells were adoptively transferred into WT mice infected with vaccinia-OVA, and a cohort of mice that received T-*Tsc2*$^{-/-}$ OT-I$^+$ cells was treated daily with 100 μg/kg rapamycin, starting on day 5 after infection. Treatment with rapamycin markedly enhanced the survival of antigen-specific T-*Tsc2*$^{-/-}$ CD8$^+$ T cells 21 days following infection (Figure 6, A and B). The increase in survival was associated with an increase in the expression of CD127

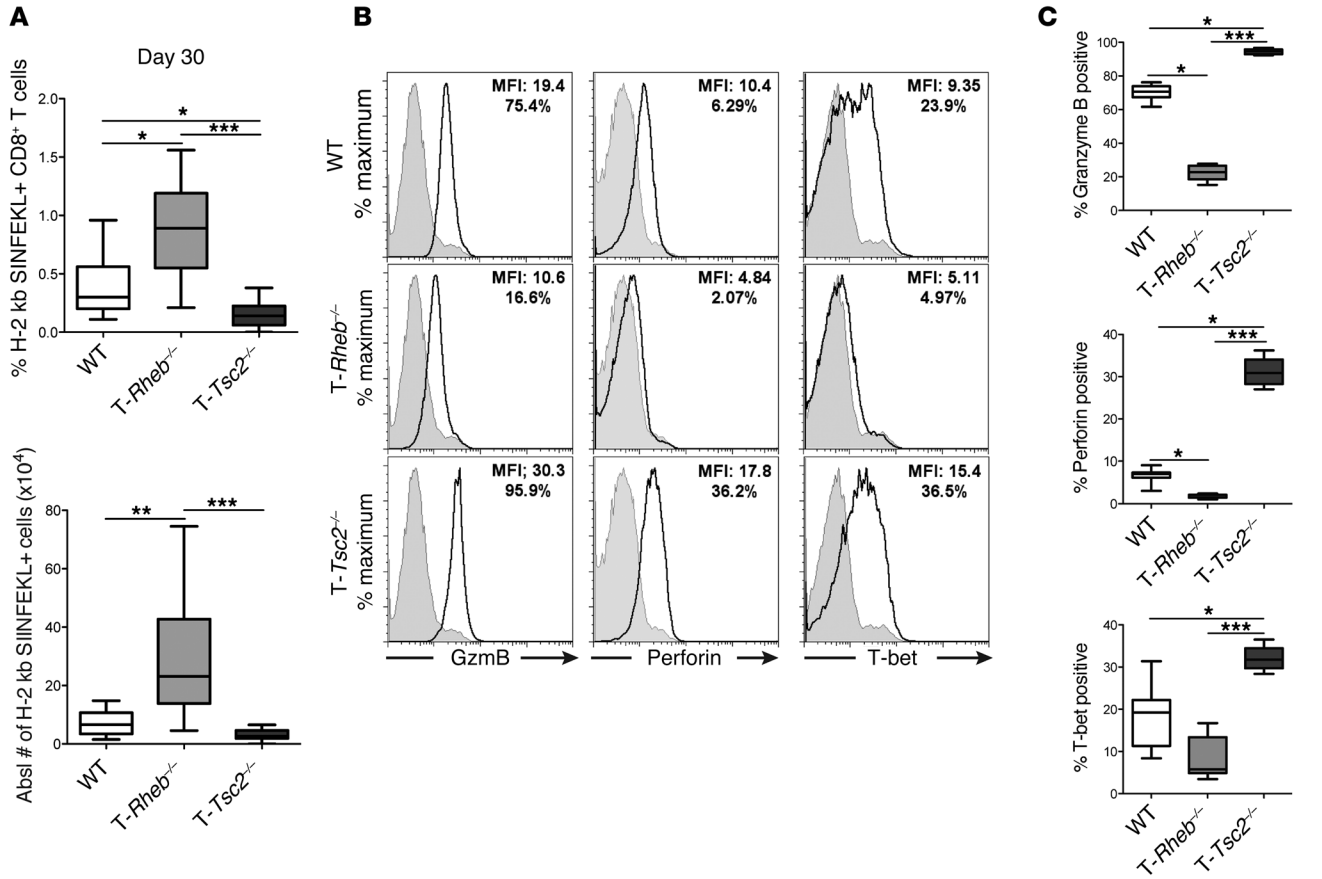

Figure 5. TSC2 inhibition results in terminally differentiated effector cells. WT, T-*Rheb*$^{-/-}$, and T-*Tsc2*$^{-/-}$ mice were infected with vaccinia-OVA. Thirty days after infection splenocytes were harvested and (**A**) percentage and absolute number of antigen-specific splenocytes were determined by H-2 kb/SIINFEKL staining of CD44$^+$CD8$^+$ cells (n = 15). For the box-and-whiskers plots, the whiskers represent the minimum and maximum values, the box boundaries represent the 25th and 75th percentiles, and the middle line is the median value. (**B**) Splenocytes from day 30 infected mice were stimulated with SIINFEKL peptide, and cytolytic and T-bet protein expression were measured. Plots are gated from the CD8$^+$ population. Shaded histograms show isotype controls. (**C**) Statistics for **B** (n = 9). Data are representative of at least 3 independent experiments. *P < 0.05, **P < 0.01, ***P < 0.001, ANOVA.

and eomesodermin, a transcription factor associated with CD8$^+$ memory (ref. 29 and Figure 6, C and D). Consistent with the role of mTORC1 in enhancing effector cell generation, this treatment also led to a decrease in KLRG1 and T-bet expression in T-*Tsc2*$^{-/-}$ OT-I$^+$ cells (Figure 6, A–D). Importantly, rapamycin treatment also promoted an enhanced recall response of T-*Tsc2*$^{-/-}$ OT-I$^+$CD8$^+$ T cells to a secondary infection with listeria-OVA (lm-OVA) (Figure 6E). This recall response was not observed in mice given T-*Tsc2*$^{-/-}$ cells without rapamycin. Thus, temporarily blocking mTORC1 activity in T-*Tsc2*$^{-/-}$ CD8$^+$ T cells promotes the generation of functional memory T cells.

TSC2 regulates the activation-induced metabolic switch in T cells. We next assessed the metabolic flux of activated CD8$^+$ T cells from WT, T-*Tsc2*$^{-/-}$, and T-*Rheb*$^{-/-}$ mice. T-*Tsc2*$^{-/-}$ CD8$^+$ T cells demonstrated a high extracellular acidification rate (ECAR), indicative of increased glycolysis, compared with WT T cells (Figure 7A). In support of this high glycolytic rate, activated T-*Tsc2*$^{-/-}$ cells have enhanced transcript expression of *Slc2a1* (the glucose transporter GLUT1) and the key glycolytic enzyme phosphofructokinase (*Pfk1*) (Figure 7B). In contrast, T-*Rheb*$^{-/-}$ T cells demonstrated markedly decreased glycolytic activity and diminished expression of *Slc2a1* and *Pfk1*. However, T-*Rheb*$^{-/-}$ CD8$^+$ T cells have an increased spare respiratory capacity (SRC), an indicator of mitochondrial energy potential associated with long-term cellular survival (Figure 7C) (6). In support of this finding, previously activated T-*Rheb*$^{-/-}$ CD8$^+$ T cells exhibited the highest mitochondrial mass, as indicated by MitoTracker Green staining (Figure 7D). Furthermore, T-*Rheb*$^{-/-}$ CD8$^+$ T cells demonstrated a increase in expression of carnitine palmitoyltransferase 1 α (*Cpt1a*), the rate-limiting step of FAO (30, 31), which is also associated with the development of memory CD8$^+$ T cells (ref. 6 and Figure 7E). In contrast, T-*Tsc2*$^{-/-}$ CD8$^+$ T cells have the lowest SRC, mitochondrial mass, and *Cpt1a* expression (Figure 7, C–E). Thus, these data indicate that mTORC1 activity is a rheostat for CD8$^+$ metabolic function. *Tsc2* deletion results in enhanced glycolytic metabolism at the expense of oxidative phosphorylation, while loss of mTORC1 activity decreases glycolysis but promotes oxidative phosphorylation and FAO.

To determine whether the enhanced effector function of T-*Tsc2*$^{-/-}$ CD8$^+$ T cells is dependent on an enhanced glycolytic metabolism, we assessed T-*Tsc2*$^{-/-}$ effector function in vivo after daily treatment with 2-deoxy-D-glucose (2DG), an inhibitor of glycolysis (32). 2DG treatment greatly reduced the percentage of

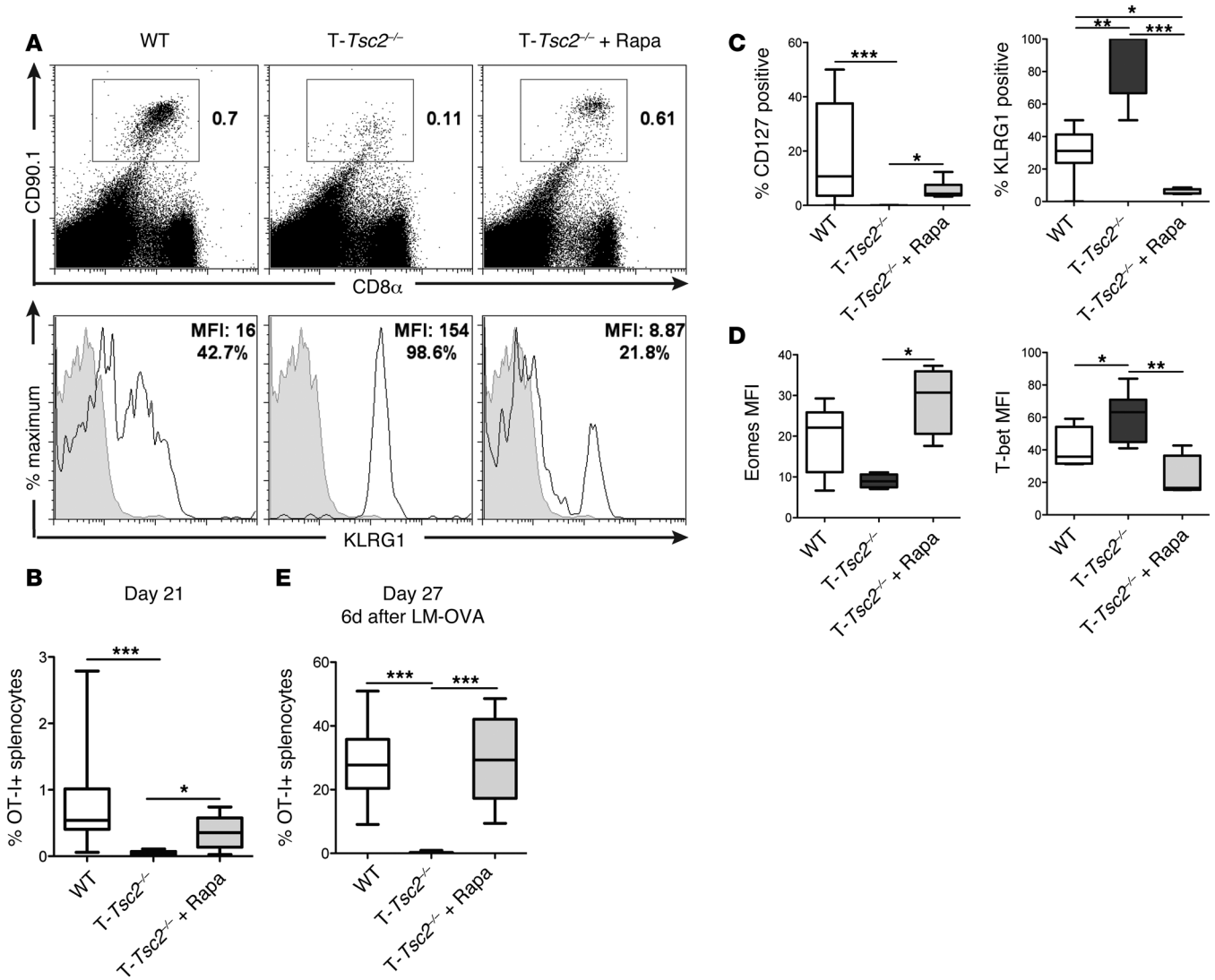

Figure 6. Rapamycin treatment can rescue the terminal effector differentiation of T-*Tsc2*$^{-/-}$ CD8$^+$ T cells. WT and T-*Tsc2*$^{-/-}$OT-I$^+$CD8$^+$CD90.1$^+$ T cells were adoptively transferred into WT CD90.2$^+$ recipients infected with vaccinia-OVA. A cohort of mice that received T-*Tsc2*$^{-/-}$ cells was treated with rapamycin. (**A**) FACS plots depict the percentage of splenic CD8$^+$CD90.1$^+$ (OT-I$^+$) cells 21 days after infection (top). KLRG1 expression of gated CD90.1$^+$ cells (bottom). Gray histogram depicts isotype control. (**B**) The percentage of recovered OT-I$^+$ splenocytes 21 days after infection (n = 8). (**C** and **D**) Phenotypic analysis of recovered OT-I$^+$ splenocytes demonstrating (**C**) changes in surface marker expression and (**D**) transcription factor expression between genotypes with or without rapamycin treatment (n = 8). (**E**) Recipient mice were infected with lm-OVA on day 21 after transfer. Six days after secondary infection with lm-OVA (day 27), splenocytes were harvested and the percentage of OT-I$^+$ splenocytes was determined (n = 14). Data are representative of 3 independent experiments. For the box-and-whiskers plots, the whiskers represent the minimum and maximum values, the box boundaries represent the 25th and 75th percentiles, and the middle line is the median value. *P < 0.05, **P < 0.01, ***P < 0.001, ANOVA. Eomes, eomesodermin.

recovered T-*Tsc2*$^{-/-}$ OT-I$^+$CD8$^+$ T cells and the IFN-γ production of OT-I$^+$ T cells after vaccinia-OVA infection, thus proving a correlation between glycolytic metabolism and T-*Tsc2*$^{-/-}$ CD8$^+$ T cell effector response (Figure 7F).

In as much as rapamycin was able to enhance memory generation in the T-*Tsc2*$^{-/-}$ CD8$^+$ T cells, we next examined the effect of rapamycin on metabolism. Rapamycin treatment reduced glycolysis, as measured by ECAR, in T-*Tsc2*$^{-/-}$ CD8$^+$ T cells (Figure 7G). This finding was associated with a decrease in *Slc2a1* and *Pfk1* (Figure 7H). In contrast, rapamycin promoted enhanced SRC (Figure 7I and Supplemental Figure 6A) and increased expression of *Cpt1a* in WT and T-*Tsc2*$^{-/-}$ CD8$^+$ T cells (Figure 7J and Supplemental Figure 6B). Thus, inhibition of mTORC1 through rapamycin treatment decreases the glycolytic metabolism of activated T-*Tsc2*$^{-/-}$ cells, enabling the generation of memory cells.

A novel role for mTORC2 in regulating CD8$^+$ T cell memory. We next wanted to determine whether mTORC2 activity is important for regulating CD8$^+$ T cell fate decisions. To this end, we used mice in which RICTOR, a critical component of mTORC2, is conditionally deleted in T cells (*Cd4-Cre Rictor*$^{fl/fl}$ mice, herein referred to as T-*Rictor*$^{-/-}$ mice). Upon TCR stimulation, T-*Rictor*$^{-/-}$ CD8$^+$ T cells have intact, if not slightly elevated, mTORC1 activity, consistent with the release of a mTORC2 feedback loop (33), and decreased mTORC2 activity (Figure 8A and Supplemental Figure 7A).

T-*Rictor*$^{-/-}$ CD8$^+$ T cells have proliferative capacity and cytokine production equivalent to those of WT cells (Supplemental

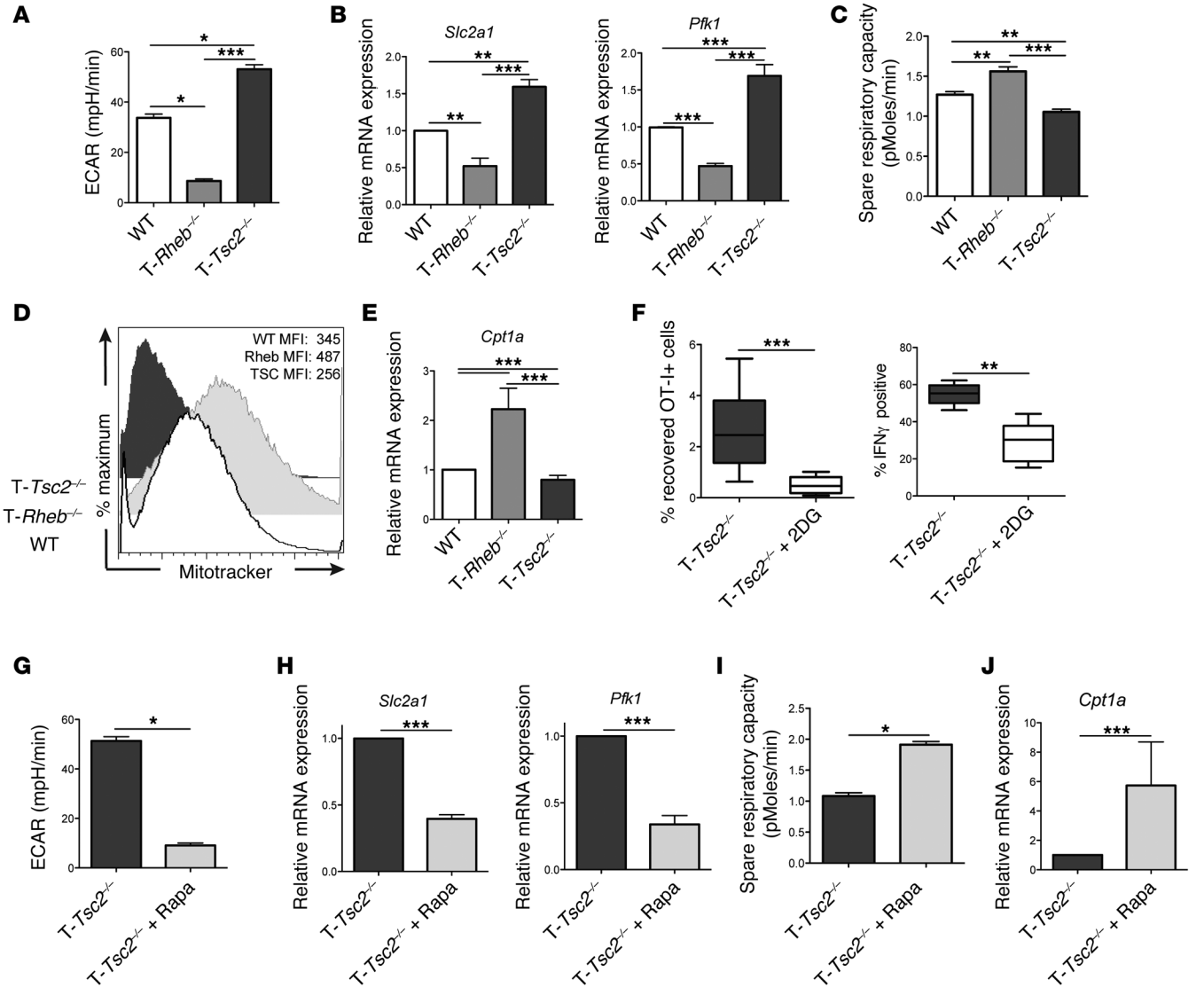

Figure 7. mTORC1 activity influences CD8⁺ T cell metabolism upon TCR stimulation. (**A**–**E**) Purified CD8⁺ T cells from WT, T-*Rheb*$^{-/-}$, and T-*Tsc2*$^{-/-}$ mice were stimulated in vitro for 48 hours and cultured in IL-7 and IL-15 for 3 days. (**A**) Cells were run on an extracellular flux analyzer, and ECAR was determined. Data are mean ± SEM of 7 measurements. (**B**) RNA was extracted and relative expression of GLUT1 (*Slc2a1*) and *Pfk1* transcripts was determined by qPCR. (**C**) As in **A**, SRC was determined. (**D**) MitoTracker Green staining was assessed by flow cytometry. (**E**) As in **B**, *Cpt1a* expression was measured. (**F**) T-*Tsc2*$^{-/-}$ OT-I⁺ T cells were transferred into congenically distinct recipients infected with vaccinia-OVA. A cohort of mice received 2DG daily. On day 6, splenocytes were harvested and the percentage of OT-I⁺ cells (n = 9) and percentage of IFN-γ–positive OT-I⁺ cells was determined after SIINFEKL stimulation (n = 5). For the box-and-whiskers plots, the whiskers represent the minimum and maximum values, the box boundaries represent the 25th and 75th percentiles, and the middle line is the median value. (**G**–**J**) Purified T-*Tsc2*$^{-/-}$CD8⁺ T cells were stimulated in vitro for 48 hours with or without 0.5 μM rapamycin. Cells were expanded in media supplemented with IL-7 and IL-15 with or without 0.5 μM rapamycin for 3 days. (**G**) As in **A**, ECAR was measured. Data are mean ± SEM of 4 measurements. (**H**) As in **B**, relative expression of S*lc2a1* and *Pfk1* transcript was detected. (**I**) As in **G**, SRC was determined, and (**J**) relative expression of *Cpt1a* transcript was measured. Statistics for **A**–**E** were determined by ANOVA and those for **F**–**J** were measured by Mann-Whitney t tests. Data are representative of 3 independent experiments. *P < 0.05, **P < 0.01, ***P < 0.001

Figure 7B). To further understand the role of mTORC2 in CD8⁺ T cell effector function, we used the in vivo adoptive transfer model. Congenically marked WT and T-*Rictor*$^{-/-}$ OT-I⁺ T cells were adoptively transferred into recipient mice that were immediately infected with vaccinia-OVA. Unlike T cells derived from T-*Rheb*$^{-/-}$ mice, T-*Rictor*$^{-/-}$ cells generated a response to vaccinia-OVA infection similar to that of WT cells (Figure 8B). This response was observed and equivalent for antigen-specific cells derived from the blood and spleen (Supplemental Figure 7C). OVA-specific T-*Rictor*$^{-/-}$ cells expressed KLRG1 and produced robust amounts of IFN-γ and TNF-α, similar to WT cells, upon ex vivo restimulation (Figure 8C). Surprisingly, at this early time point (day 6 after infection), we also observed a substantial population of T-*Rictor*$^{-/-}$ cells expressing CD127 (Figure 8C). These findings were recapitulated after transfer of sorted naive cells. Six days after infection, transfer of naive T-*Rictor*$^{-/-}$ OT-I⁺CD8⁺ T cells resulted in equivalent,

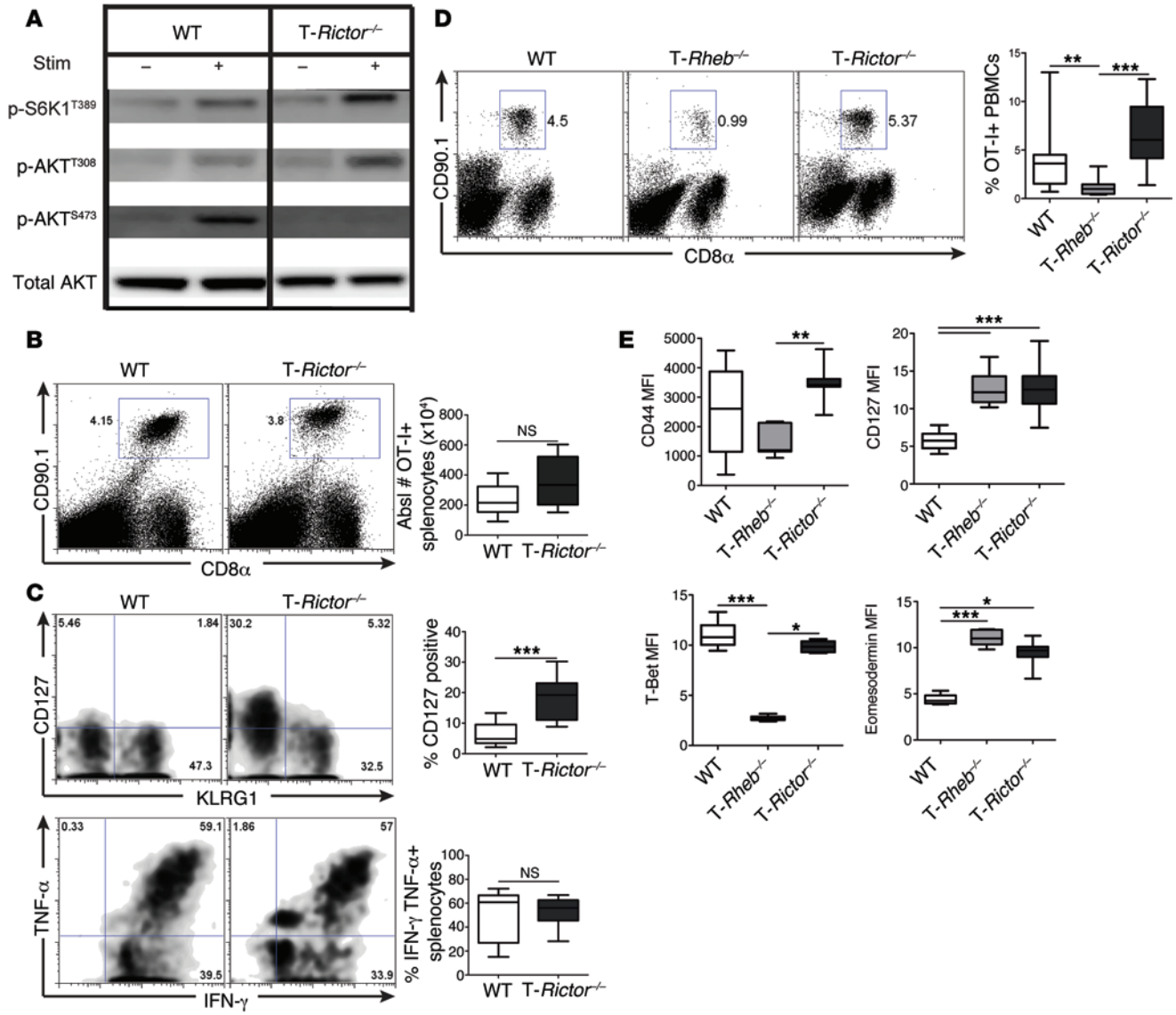

Figure 8. mTORC2 activity is not required for CD8⁺ T cell effector function. (**A**) Purified CD8⁺ T cells were collected from 6-week-old WT or T-*Rictor*$^{-/-}$ mice. mTORC1 and mTORC2 activity was assessed by immunoblot analysis from unstimulated cells or after 1-hour stimulation with αCD3/αCD28. (**B** and **C**) WT and T-*Rictor*$^{-/-}$ OT-I⁺CD8⁺CD90.1⁺ cells were adoptively transferred into WT CD90.2⁺ recipients infected with vaccinia-OVA. Six days after infection, splenocytes were harvested. (**B**) The percentage of OT-I⁺ splenocytes was determined. The graph depicts the absolute number of OT-I⁺ splenocytes (n = 12). (**C**) Surface staining of OT-I⁺ splenocytes 6 days after infection, with the percentage of recovered OT-I⁺ cells expressing CD127 (n = 12) (top). Cytokine production of OT-I⁺ splenocytes after SIINFEKL stimulation, with statistics shown to the right (n = 12) (bottom). (**D** and **E**) 1.5 × 10^5 naive sorted WT, T-*Rheb*$^{-/-}$, and T-*Rictor*$^{-/-}$ OT-I⁺CD90.1⁺ T cells were adoptively transferred into WT CD90.2⁺ recipients infected with vaccinia-OVA. (**D**) The percentage of recovered OT-I⁺ T cells was determined from blood 6 days after infection, with statistics shown to the right (n = 15). (**E**) Surface marker and transcription factor expression were assessed from recovered OT-I⁺ splenocytes (n = 9). For the box-and-whiskers plots, the whiskers represent the minimum and maximum values, the box boundaries represent the 25th and 75th percentiles, and the middle line is the median value. Statistics for **B** and **C** were determined by Mann-Whitney t tests, while those for **D** and **E** were measured by ANOVA. Data are representative of 3 independent experiments. *P < 0.05, **P < 0.01, ***P < 0.001.

if not enhanced, accumulation of antigen-specific CD8⁺ T cells compared with transfer of WT cells, while T-*Rheb*$^{-/-}$ CD8⁺ T cell transfer yielded the lowest percentage of antigen-specific CD8⁺ T cells (Figure 8D). Additionally, T-*Rictor*$^{-/-}$ CD8⁺ T cells have an activated effector phenotype similar to that of WT cells, expressing high levels of CD44 and T-bet (Figure 8E). However, T-*Rictor*$^{-/-}$ CD8⁺ T cells also have enhanced expression of CD127 and eomesodermin, which were upregulated in T-*Rheb*$^{-/-}$ CD8⁺ T cells but not WT cells at this time point after infection (Figure 8E). Furthermore, antigen-specific T-*Rictor*$^{-/-}$ cells have low levels of caspase-3 activity, similar to WT and T-*Rheb*$^{-/-}$ CD8⁺ T cells, but the highest expression of BCL-2 (Supplemental Figure 7, D and E). Thus, CD8⁺ T cells with diminished mTORC2 activity generate robust effector responses, while simultaneously expressing markers of memory.

To further investigate the longevity of T-*Rictor*$^{-/-}$ CD8⁺ T cells, we tracked the frequency of WT and T-*Rictor*$^{-/-}$ OT-I⁺ T cells for 35 days after infection in the blood (Figure 9A). By day 12, the frequency of T-*Rictor*$^{-/-}$ OT-I⁺CD8⁺ T cells was higher than that

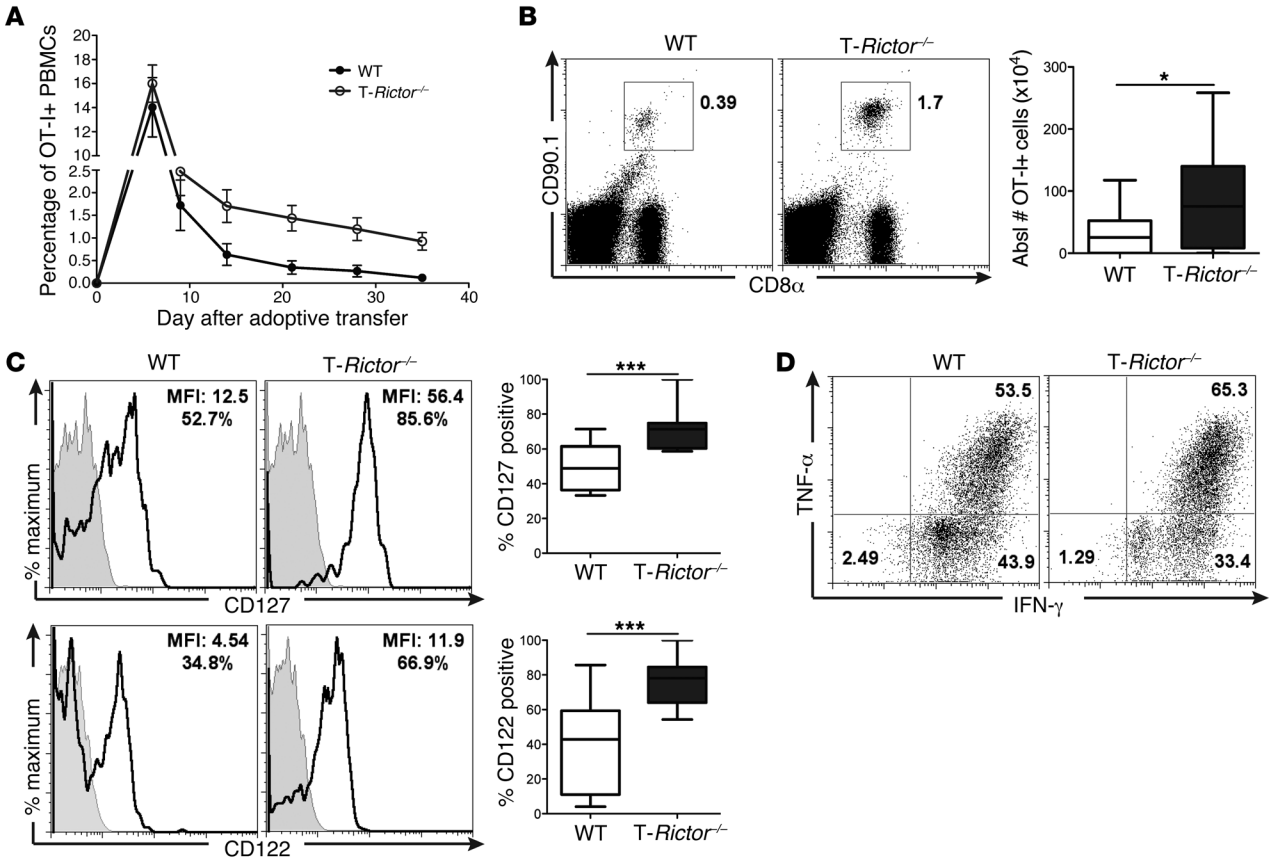

Figure 9. mTORC2 inhibition does not hinder CD8⁺ T cell acute effector function. (**A**) 1.5 × 10^5 naive sorted WT and T-*Rictor*$^{-/-}$ OT-I⁺CD8⁺CD90.1⁺ T cells were adoptively transferred into WT recipients infected with vaccinia-OVA, and the percentage of OT-I⁺ cells was monitored in the blood. The two groups are statistically significant during the memory phase, as assessed by repeated-measures analysis (see *Statistics*) (n = 9). (**B**–**D**) WT and T-*Rictor*$^{-/-}$ OT-I⁺CD8⁺CD90.1⁺ cells were adoptively transferred into WT recipients infected with vaccinia-OVA, and the number and phenotype of OT-I⁺ splenocytes were assessed 26 days after adoptive transfer and infection. (**B**) The percentage and absolute number of recovered OT-I⁺ splenocytes, and (**C**) surface marker expression of OT-I⁺ splenocytes was determined by flow cytometry. MFI and the percentage of antigen-specific cells expressing CD127 or CD122 are shown in plots. Gray histograms depict isotype controls (n = 12). (**D**) 26 days after infection, mice were given a secondary infection with lm-OVA, and 6 days later cytokine production of OT-I⁺ splenocytes was determined. For the box-and-whiskers plots, the whiskers represent the minimum and maximum values, the box boundaries represent the 25th and 75th percentiles, and the middle line is the median value. Statistics in **A** were determined by repeated-measures analysis and those in **B** and **C** were measured by Mann-Whitney t tests. Data are representative of at least 3 independent experiments. *P < 0.05, ***P < 0.001.

of WT cells. Further assessment of splenocytes 26 days after infection revealed an increased frequency of T-*Rictor*$^{-/-}$ OT-I⁺ T cells compared with that of WT cells (Figure 9B). These cells expressed higher levels of the memory cell markers CD127 and CD122 (IL-2R/15Rβ) than WT T cells (Figure 9C). Thus, T-*Rictor*$^{-/-}$ CD8⁺ T cells have a survival advantage over memory cells generated from WT mice.

Having demonstrated that T-*Rictor*$^{-/-}$ T cells have prolonged survival with increased markers of memory CD8⁺ T cells, we next assessed their ability to respond upon rechallenge. To this end, 26 days after adoptive transfer and infection with vaccinia-OVA, recipient mice were rechallenged with lm-OVA, and the WT and T-*Rictor*$^{-/-}$ OT-I⁺ T cell response was determined 6 days later. T-*Rictor*$^{-/-}$ T cells demonstrated robust production of IFN-γ and TNF-α upon ex vivo stimulation (Figure 9D). Additionally, the enhanced generation of long-lived memory cells by T-*Rictor*$^{-/-}$ OT-I⁺ T cells was observed after rechallenge with lm-OVA 133 days after initial infection (Figure 10, A and B). To further demonstrate the enhanced ability of the T-*Rictor*$^{-/-}$ T cells to generate memory cells, we sorted WT and T-*Rictor*$^{-/-}$ OT-I⁺ T cells from mice 35 days after infection (Figure 10, C and D) and performed a second adoptive transfer of equivalent cell number into naive recipients. Infection of these mice with vaccinia-OVA resulted in enhanced expansion of the T-*Rictor*$^{-/-}$ OT-I⁺ T cells when compared with the adoptively transferred WT T cells (Figure 10D). Thus, T cells lacking mTORC2 signaling not only demonstrate enhanced differentiation into memory cells but also generate elevated responses upon rechallenge.

We consistently found that long-lived T-*Rictor*$^{-/-}$ CD8⁺ T cells expressed increased levels of CD127, CD62L, and eomesodermin (Figure 8E and Figure 10E). The expression of these molecules is controlled in part by the transcription factor, FOXO1 (34). Phosphorylation of FOXO1 results in cytoplasmic retention and hence inhibits its function. This phosphorylation has previously been shown to be regulated in part by mTORC2 activity (35). Thus, we hypothesized that the deletion of RICTOR could enhance the generation of memory T cells in part by increasing the retention of FOXO1 in the nucleus. Consistent with this

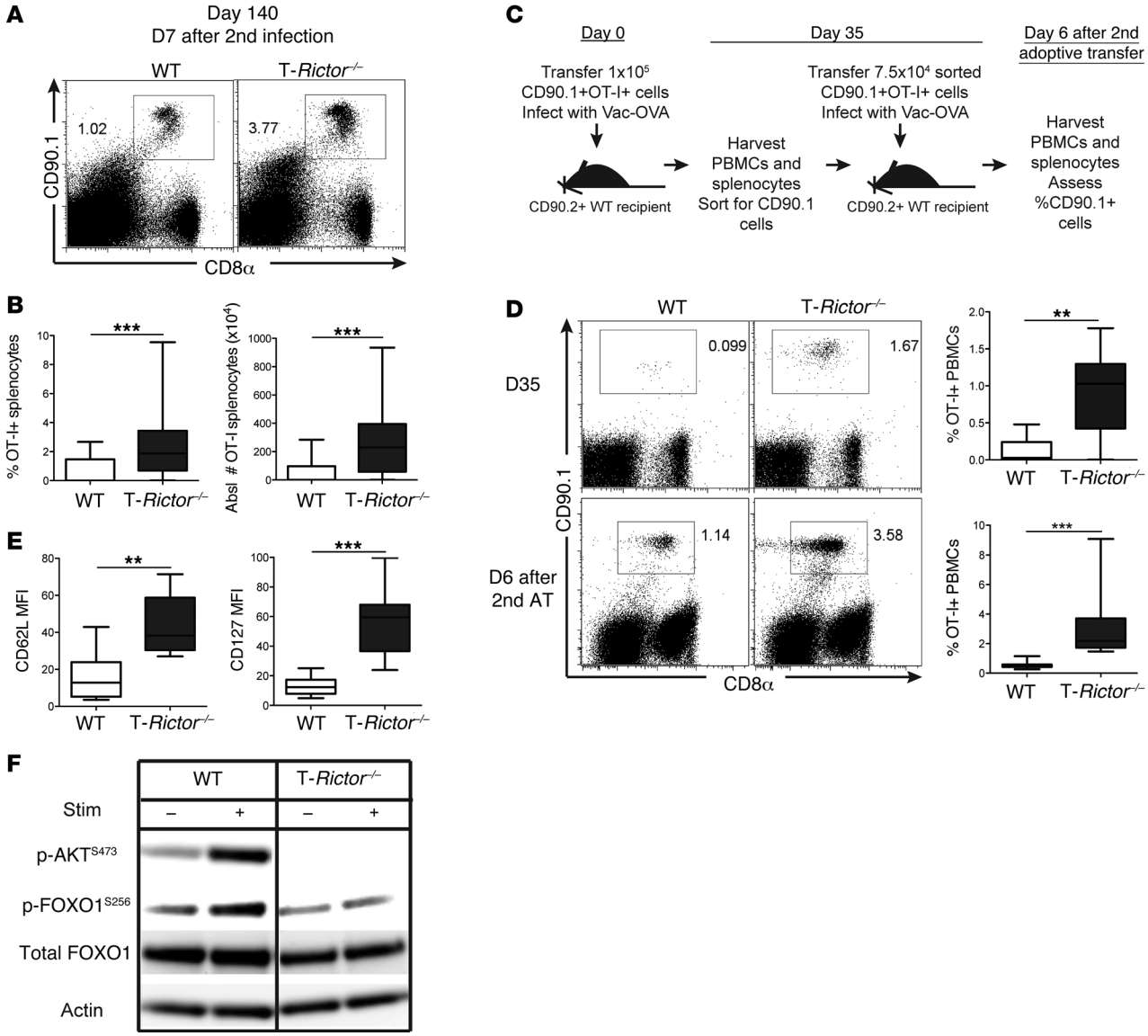

Figure 10. mTORC2 inhibition promotes memory generation. (**A**–**E**) 1.5 × 10^5 naive sorted OT-I$^+$ T cells were transferred into WT CD90.2$^+$ recipients infected with vaccinia-OVA. (**A** and **B**) Mice were given secondary infection of Im-OVA 133 days after initial infection, and 7 days later, the percentage and absolute number of recovered OT-I$^+$ splenocytes was determined (n = 20). (**C**) Experimental schematic for **D**. (**D**) Flow cytometric analysis of the percentage of OT-I$^+$ cells recovered from blood 35 days after primary infection, with statistics shown on the right (n = 9) (top). OT-I$^+$ cells were purified after harvest on day 35, transferred into new recipients infected with vaccinia-OVA, and 6 days later, percentage of OT-I$^+$ PBMCs was determined (labeled as "D6 after 2nd AT"), with statistics shown to the right (n = 7) (bottom). (**E**) CD62L and CD127 expression of recovered OT-I$^+$ splenocytes 35 days after primary infection (n = 9). (**F**) p-FOXO1 protein expression was detected from in vitro–stimulated and IL-7– and IL-15–expanded CD8$^+$ T cells with or without restimulation. Data are representative of at least 3 independent experiments. For the box-and-whiskers plots, the whiskers represent the minimum and maximum values, the box boundaries represent the 25th and 75th percentiles, and the middle line is the median value. $^{**}P < 0.01$, $^{***}P < 0.001$, Mann-Whitney t tests.

mechanism, FOXO1 phosphorylation was diminished in activated T-*Rictor*$^{-/-}$ CD8$^+$ T cells (Figure 10F). Of note, in spite of their ability to generate robust memory responses, T-*Rictor*$^{-/-}$ T cells were no better at acutely rejecting tumors than WT T cells (Supplemental Figure 7, F and G).

Inhibition of mTORC2 promotes metabolism associated with both effector and memory CD8$^+$ T cells. Next, we sought to determine whether the ability of mTORC2 to regulate memory cell generation was also linked to metabolism. WT and T-*Rictor*$^{-/-}$ CD8$^+$ T cells were stimulated in vitro and expanded in the presence of IL-2 (to promote effector formation) or IL-7 and IL-15 (to promote memory differentiation) (6, 36). Regardless of the cytokine milieu, T-*Rictor*$^{-/-}$ CD8$^+$ T cells demonstrated a marked increase in ECAR, indicative of a glycolytic metabolism when compared with WT T cells (Figure 11A). That is, even under in vitro conditions that mimic memory generation, the T-*Rictor*$^{-/-}$ CD8$^+$ T cells have increased glycolytic flux. Additionally, the initial oxygen consumption rate (OCR) was elevated in T-*Rictor*$^{-/-}$ cells when compared with that in WT T cells in both the effector and memory culture conditions (Figure 11A). Furthermore, while WT and T-*Rictor*$^{-/-}$ cells have a similar SRC after culture in IL-7 and IL-15, culture in IL-2 did not diminish the SRC of

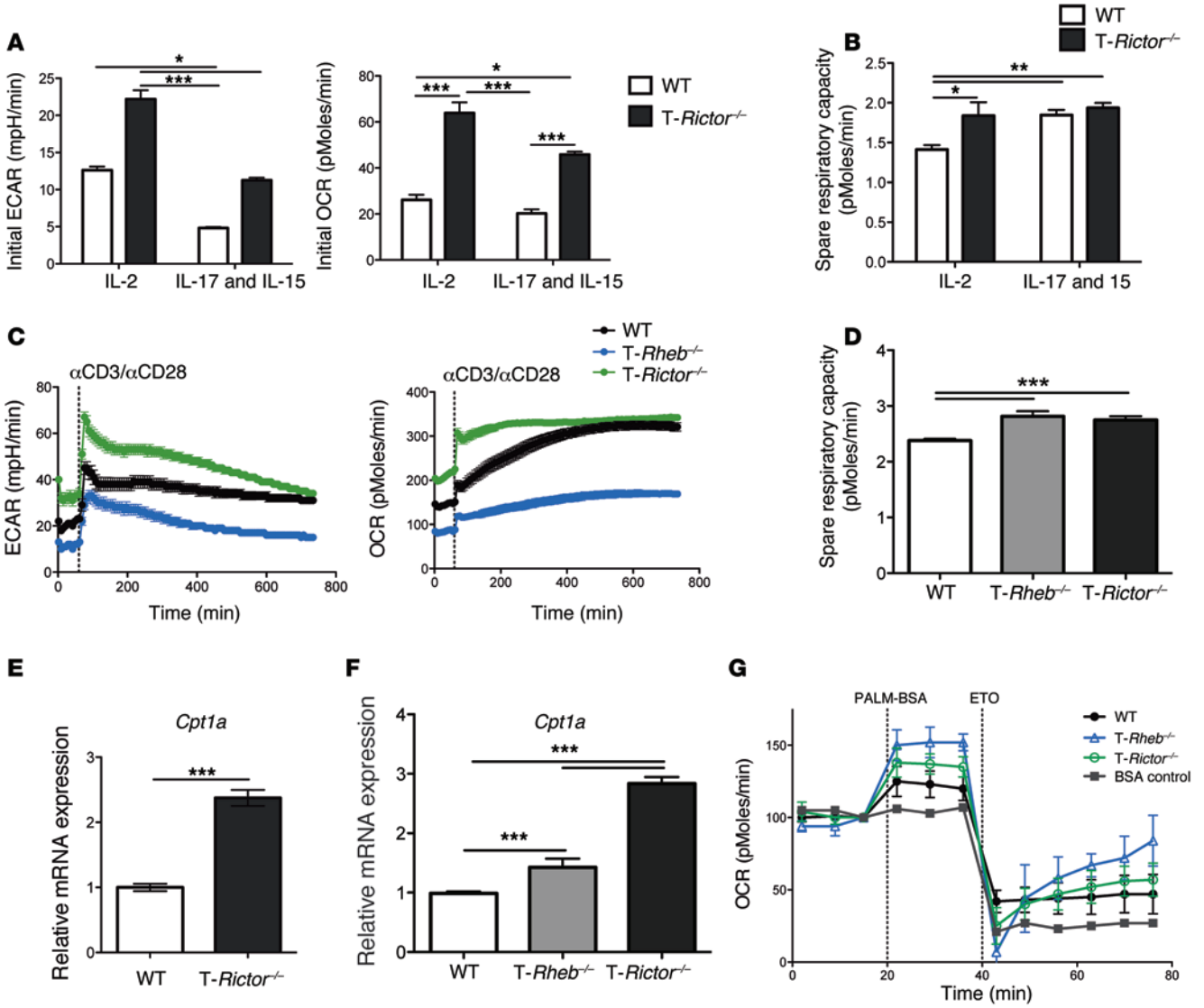

Figure 11. mTORC2 inhibition leads to enhanced metabolic fitness. Purified CD8⁺ T cells from WT or T-*Rictor*$^{-/-}$ mice were stimulated in vitro for 48 hours and expanded for 3 days. (**A**) Initial ECAR, initial OCR, and (**B**) SRC were determined. Data are mean ± SEM of 7 measurements. (**C**) WT, T-*Rheb*$^{-/-}$, and T-*Rictor*$^{-/-}$ CD8⁺ T cells were stimulated in vitro and cultured in IL-7 and IL-15 for 3 days. Cells were plated at equivalent cell number, and ECAR and OCR measurements were assayed upon stimulation in the Seahorse bioanalyzer. Data are mean ± SEM of 12 measurements. (**D**) SRC was determined after restimulation of WT, T-*Rheb*$^{-/-}$, and T-*Rictor*$^{-/-}$ CD8⁺ T cells expanded in IL-7 and IL-15. Data are mean ± SEM of 10 measurements. Relative expression of *Cpt1a* transcript was determined from (**E**) stimulated cells expanded in IL-7 and IL-15 for 3 days (mean ± SEM of 3 measurements) or from (**F**) sorted WT, T-*Rheb*$^{-/-}$, and T-*Rictor*$^{-/-}$ OT-I⁺ cells recovered 6 days after adoptive transfer into recipients infected with vaccinia-OVA (n = 3 mice per genotype). (**G**) OCR measurements of restimulated WT, T-*Rheb*$^{-/-}$, and T-*Rictor*$^{-/-}$CD8⁺ T cells during a FAO assay. BSA control shown in gray. Data are mean ± SEM of 4 measurements. Statistics in **A**, **B**, **D**, and **F** were determined by ANOVA; those in **C** were measured by repeated-measures analysis; and those in **E** were measured by Mann-Whitney t test. Data are representative of at least 3 independent experiments. For the box-and-whiskers plots, the whiskers represent the minimum and maximum values, the box boundaries represent the 25th and 75th percentiles, and the middle line is the median value. *P < 0.05, **P < 0.01, ***P < 0.001.

T-*Rictor*$^{-/-}$ CD8⁺ T cells (Figure 11B). Therefore, under conditions that promote glycolysis and effector generation, T-*Rictor*$^{-/-}$ T cells still maintain a high SRC, which is associated with the development of memory.

Unlike the T-*Rictor*$^{-/-}$ T cells, the T-*Rheb*$^{-/-}$ T cells fail to respond upon rechallenge. We hypothesized that this might be due to the differences in the ability of T-*Rheb*$^{-/-}$ and T-*Rictor*$^{-/-}$ memory CD8⁺ T cells to upregulate metabolic programs upon rechallenge. To this end, WT, T-*Rheb*$^{-/-}$, and T-*Rictor*$^{-/-}$ CD8⁺ T cells were stimulated, cultured in IL-7 and IL-15, and then rechallenged with αCD3/αCD28, while simultaneously measuring ECAR and OCR. T-*Rictor*$^{-/-}$ CD8⁺ T cells displayed increased ECAR and OCR both at baseline and after restimulation (Figure 11C). In contrast, consistent with their inability to mount an effector response upon rechallenge, T-*Rheb*$^{-/-}$ T cells failed to increase glycolytic flux (Figure 11C). However, both T-*Rictor*$^{-/-}$ and T-*Rheb*$^{-/-}$ CD8⁺ T cells have increased SRC when compared with that of WT T cells (Figure 11D). Furthermore, both T-*Rictor*$^{-/-}$ and T-*Rheb*$^{-/-}$ CD8⁺ T cells expressed increased levels of *Cpt1a* after either in vitro or in vivo stimulation (Figure 7E and

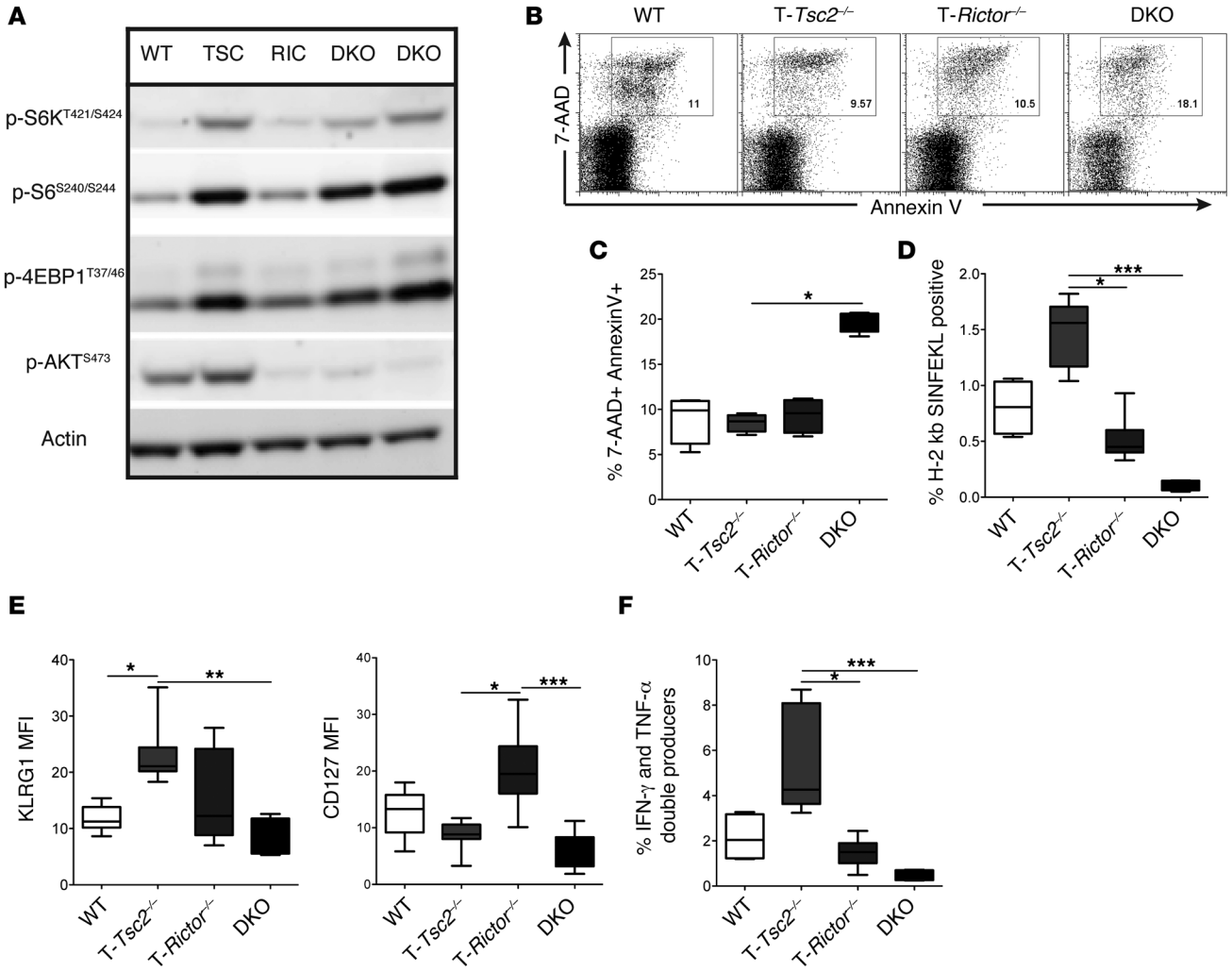

Figure 12. Inhibition of mTORC2 in the presence of hyperactive mTORC1 leads to enhanced cellular death. (**A**) Purified CD8$^+$ T cells from WT, T-*Tsc2*$^{-/-}$, T-*Rictor*$^{-/-}$, and DKO mice were stimulated in vitro for 1 hour, and mTORC1 and mTORC2 activity was assessed by immunoblot. (**B**) Splenocytes from WT, T-*Tsc2*$^{-/-}$, T-*Rictor*$^{-/-}$, and DKO mice were stimulated in vitro for 24 hours prior to analysis of CD8$^+$ T cell death by 7-AAD and annexin V staining. (**C**) Statistics for **B** (n = 4). (**D**–**F**) Mice of each genotype were infected with vaccinia-OVA. Six days later, (**D**) the percentage of antigen-specific CD44$^+$CD8$^+$ splenocytes and (**E**) surface marker expression of the antigen-specific CD8$^+$ T cells were determined. (**F**) Cytokine production was assessed after ex vivo stimulation of splenocytes gated from CD44$^+$CD8$^+$ cells (n = 6). Data are representative of 3 independent experiments. For the box-and-whiskers plots, the whiskers represent the minimum and maximum values, the box boundaries represent the 25th and 75th percentiles, and the middle line is the median value. *P < 0.05, **P < 0.01, ***P < 0.001, ANOVA.

Figure 11, E and F). This correlated with an increase in OCR in response to palmitate, indicating that activated T-*Rictor*$^{-/-}$ and T-*Rheb*$^{-/-}$ CD8$^+$ T cells can use FAO as an energy source (Figure 11G). Thus, loss of mTORC2 signaling promotes the upregulation of metabolic machinery necessary for development of both effector and memory responses.

Finally, we have consistently found that T cell–specific deletion of *Tsc2* results in hyperactivated CD8$^+$ T cells that have enhanced proliferation, cytokine secretion, and killing responses. However, these results are dramatically distinct from previously published findings with TSC1-deficient CD8$^+$ T cells (13–16, 37). We thus speculated that the differences between the T-*Tsc1*$^{-/-}$ and T-*Tsc2*$^{-/-}$ CD8$^+$ T cells might be accounted for in part by the presence or absence of mTORC2 activity. Recall that, unlike T-*Tsc1*$^{-/-}$ T cells, T-*Tsc2*$^{-/-}$ CD8$^+$ T cells have relatively intact mTORC2 signaling (Figure 1A and Figure 2B) (13, 14, 16). To this end, we crossed T-*Tsc2*$^{-/-}$ mice with T-*Rictor*$^{-/-}$ mice to generate T-*Tsc2*$^{-/-}$ *Rictor*$^{-/-}$ (*Cd4-Cre Tsc2*$^{fl/fl}$ *Rictor*$^{fl/fl}$, double-knockout [DKO]) mice. DKO mice have hyperactive mTORC1 signaling but ablated mTORC2 activation (Figure 12A). DKO cells have elevated activation-induced death compared with WT, T-*Tsc2*$^{-/-}$, and T-*Rictor*$^{-/-}$ CD8$^+$ T cells stimulated in vitro (Figure 12, B and C). We infected WT, T-*Tsc2*$^{-/-}$, T-*Rictor*$^{-/-}$, and DKO mice with vaccinia-OVA and assessed effector responses 6 days later. Similar to the reported T-*Tsc1*$^{-/-}$ T cells (13–16, 37), T cells lacking both TSC2 and RICTOR demonstrated decreased expansion in response to antigen, decreased KLRG1 and CD127 upregulation, and decreased cytokine production (Figure 12, D–F). Thus, we conclude that intact mTORC2 activity is critical for the hyperactive effector response detected in T-*Tsc2*$^{-/-}$ mice and further explains the difference in phenotype between T-*Tsc1*$^{-/-}$ and T-*Tsc2*$^{-/-}$ CD8$^+$ T cells.

Discussion

Upon antigen recognition, naive CD8$^+$ T cells undergo tremendous proliferation, leading to the generation and activation of effector CTLs (1). Recent studies emphasize that a critical aspect of effector generation is the upregulation of metabolic programs that help fuel this response (38, 39). In this regard, T cells integrate a vast array of signals from the immune microenvironment in order to coordinate the outcome of antigen recognition with the proper metabolic programs necessary to sustain such a response (7). TSC2 is a critical inhibitor of mTORC1 activation, which is inactivated by PI3-kinase–mediated signaling (40). In this report, we identify TSC2 as a key integrator of CD8$^+$ immune function and metabolism. T-*Tsc2*$^{-/-}$ CD8$^+$ T cells demonstrate superior effector function when compared with WT T cells. This was observed in experiments using both previously activated and naive T-*Tsc2*$^{-/-}$ CD8$^+$ T cells. Alternatively, by promoting a glycolytic program necessary for effector cell differentiation and function, the absence of TSC2 precludes the generation of long-lived memory T cells.

TSC2 and TSC1 form the tuberous sclerosis complex, which serves to inhibit mTORC1 by acting as a GAP for RHEB (10). There have been several reports defining the role of TSC1 in CD8 T cell function and survival (13–16, 37, 41). Both TSC1 and TSC2 deficiency result in a reduction of peripheral CD8$^+$ T cells and enhanced antigen-independent activation and proliferation (13–15). However, while *Tsc1*$^{-/-}$ mice have poor CD8$^+$ T cell responses, demonstrated by a reduction of antigen-specific CD8$^+$ T cells, and less IFN-γ and TNF-α secretion in response to ex vivo stimulation (14, 37), T-*Tsc2*$^{-/-}$ mice have enhanced CD8$^+$ T cell effector responses, thus allowing for enhanced acute tumor clearance. Of note, differences between the roles of TSC1 and TSC2 in other cell types are not without precedent (42–45). Mechanistically, the reduction of CD8 T cell responses in *Tsc1*$^{-/-}$ mice is thought to be due to increased cellular death resulting from decreased BCL-2 expression as well as abnormal mitochondrial potential and increased reactive oxygen species (13–16). Importantly, we did not observe a decrease in the antiapoptotic molecules BCL-2 or BCL-XL or an increase in TCR-induced cell death in T-*Tsc2*$^{-/-}$ CD8$^+$ T cells. Notably, T-*Tsc1*$^{-/-}$ T cells demonstrate marked diminution in mTORC2 activity, as measured by phosphorylation of AKT (S473) (13, 14, 16). In contrast, we did not observe significant defects in mTORC2 signaling in the T-*Tsc2*$^{-/-}$ cells. To determine whether mTORC2 activation is necessary for the enhanced effector function observed in the T-*Tsc2*$^{-/-}$ cells, we crossed T-*Tsc2*$^{-/-}$ mice with T-*Rictor*$^{-/-}$ mice to generate DKO mice. Interestingly, DKO mice lose the enhanced CD8$^+$ T cell effector capacities observed in T-*Tsc2*$^{-/-}$ mice and, additionally, have a reduction the CD127 expression demonstrated in T-*Rictor*$^{-/-}$ mice. This latter finding is of interest in light of the more recent work demonstrating a role for TSC1 in memory T cell formation (37, 41).

Metabolically, activated T cells demonstrate increased glycolysis (4). It is thought that by using this relatively inefficient means of generating energy, T cells (and cancer cells) are able to generate important substrates necessary for proliferation (4). Indeed, T-*Tsc2*$^{-/-}$ CD8$^+$ T cells demonstrate increased glycolysis. We propose that TSC2 controls glycolysis in part by its ability to inhibit mTORC1 (7, 46). Our observations that T-*Rheb*$^{-/-}$ T cells, which have markedly diminished mTORC1 activity, exhibited diminished glycolysis and failed to become effector cells are consistent with these findings. These results corroborate recent work, which demonstrates impaired effector function and glycolytic metabolism in RAPTOR-deficient CD8$^+$ T cells (47). Importantly, we observed that antigen-experienced T-*Rheb*$^{-/-}$ T cells, which display a memory phenotype, also failed to mount a robust effector response upon rechallenge. That is, mTORC1 activity is not only necessary for the initial differentiation into effector cells but is also important for the generation of an effector response derived from memory cells.

The metabolic demands of CD8$^+$ memory T cells differ greatly from those of effector cells (6). Rather than using glycolysis, memory cells are much more dependent on fatty acid oxidation (FAO), and their long-term survival is promoted by an increased mitochondrial SRC (6, 48). Along these lines, we demonstrated decreased FAO and SRC in the T-*Tsc2*$^{-/-}$ CD8$^+$ T cells. Thus, we hypothesize that the increase in CD8$^+$ T cell activation, combined with the decrease in metabolic reprogramming necessary for long-term survival, explains the overall reduction of peripheral CD8$^+$ T cells observed in the T-*Tsc2*$^{-/-}$ mice. On the other hand, treatment with the mTORC1 inhibitor, rapamycin, restored the ability of the T-*Tsc2*$^{-/-}$ CD8$^+$ T cells to differentiate into memory T cells. The ability of rapamycin to promote memory generation in the T-*Tsc2*$^{-/-}$ mice was associated with a decrease in glycolysis and an increase in the SRC. Such findings are consistent with previous reports demonstrating the ability of low-dose rapamycin to promote memory cell generation in WT mice (27, 28). Mechanistically, it was shown that rapamycin treatment augments the generation of memory cells in part by mediating a switch from expression of T-bet to eomesodermin. In addition to these immunologic programs, our data demonstrate that mTOR inhibition promotes memory cell generation by regulating metabolism as well. The consequences of these observations have begun to be exploited. It was found that rapamycin treatment could enhance the generation of memory T cells in response to vaccinia vaccination in rhesus macaques (49). Likewise, it has been shown that rapamycin can also enhance memory T cell generation in mouse models of tumor immunotherapy (28, 50, 51). Further, another report demonstrates that inhibiting glycolysis upon CD8$^+$ T cell activation enhances the generation of CD8$^+$ T cell memory, which suggests that the rescue of memory recall in T-*Tsc2*$^{-/-}$ CD8$^+$ T cells by rapamycin is in part due to decreased glycolytic function (52). Another group observed similar findings, whereby siRNA aptamer targeting of RAPTOR (downregulating mTORC1 signaling) enhanced CD8$^+$ T cell memory responses and had better therapeutic effect than rapamycin treatment in an antitumor vaccine strategy against a murine model of melanoma (53).

In light of our findings that TSC2 regulates CD8$^+$ effector cell generation in an mTORC1-dependent fashion, we wanted to determine the potential role of mTORC2 in regulating CD8$^+$ T cell effector and memory cell fates. To this end, we also examined the generation of effector and memory CD8$^+$ T cells in T-*Rictor*$^{-/-}$ mice. Unlike what we observed in T-*Rheb*$^{-/-}$ mice, the absence of mTORC2 signaling had no negative consequences for the generation of CD8$^+$ effector cells. Additionally, the generation of memory T cells in T-*Rictor*$^{-/-}$ mice was enhanced.

This enhancement was associated with increased IL-7 and IL-15 receptor expression (24, 54). The expression of both of these genes is enhanced by FOXO nuclear translocation, which in turn is blocked by mTORC2 activity (34, 55, 56). Thus, mechanistically, we propose that mTORC2 limits memory generation by mitigating FOXO-induced expression of these key cytokine receptors. Consistent with this idea, recent work has found that $CD8^+$ T cells deficient in FOXO1 are unable to transition to a memory phenotype (57, 58). Metabolically, T-*Rictor*$^{-/-}$ T cells readily mount a glycolytic response to antigen activation but also demonstrate an enhanced SRC associated with long-term survival. Likewise, T-*Rictor*$^{-/-}$ T cells exhibit high expression of *Cpt1a*, endowing them with the ability to metabolize fat-derived carbon sources. It has been reported that memory $CD8^+$ T cells have enhanced glycolytic capacity upon activation (48). In contrast to a report using pharmacologic blockade of mTOR that found that mTORC2 is required for the glycolytic switch required during the activation of memory cells, we found that genetic deletion of mTORC2 in $CD8^+$ T cells (T-*Rictor*$^{-/-}$) resulted in high ECAR prior to and upon restimulation, which was not found in mTORC1-deficient (T-*Rheb*$^{-/-}$) $CD8^+$ T cells (59). These results are consistent with a recent report demonstrating increased persistence of human tumor-infiltrating lymphocytes after pretreatment with an AKT inhibitor (resulting in reduced mTORC2 and mTORC1 activity) (60).

Similarly, our data identifying a role for mTORC2 activity in regulating memory cell generation have interesting clinical implications. Currently, the strategic use of rapamycin is being developed as a means to enhance vaccine efficacy (61). Clearly such a strategy will have to balance the inhibitory effects of rapamycin on effector function with its ability to enhance memory cell generation. Our data using T-*Rictor*$^{-/-}$ mice suggest that the selective inhibition of mTORC2 might prove to be an even more effective means of enhancing memory T cell generation, without dampening effector responses.

Methods

Mice. C57BL/6, *Cd4-Cre*, and OT-I mice were obtained from The Jackson Laboratory and bred to CD90.1 backgrounds. Mice with *lox*P-flanked *Tsc2* alleles were generated by the laboratory of Michael Gambello, University of Texas Health Science Center at Houston, Houston, Texas, USA (21). Mice with *lox*P-flanked *Rheb* alleles were generated in the laboratory of Paul Worley, Johns Hopkins University School of Medicine (23). Mice with *lox*P-flanked *Rictor* alleles were a gift from Mark Magnuson, Vanderbilt University Medical Center, Nashville, Tennessee, USA (62). Genotyping was determined from respective protocols. All mice were backcrossed on to the C57BL/6 background for 9 generations. Male and female mice were used for each experiment; mice were sex and age matched accordingly.

Antibodies and reagents. Antibodies against the following proteins were purchased from BD Biosciences: CD4 (GK1.5), CD8α (53-6.7), CD90.1 (OX-7), Vβ5.1,5.2 TCR, CD44 (IM7), IL-2 (JES6-5H4), TNF-α (MP6-XT22), IFN-γ (XMG1.2), active caspase-3, and BCL2 (K112-91). 7-AAD and annexin V were also purchased from BD Biosciences. Antibodies against the following proteins were from eBioscience: B220 (RA3-6B2), CD3e (145-2C11), CD62L (MEL-14), CD122 (TM-b1), CD127 (A7R34), T-bet (eBio4B10), eomesodermin (Dan11mag), granzyme B (NGZB), and Perforin (eBioOMAK-D). Anti-KLRG1 was obtained from Southern Biotech. The following immunoblot analysis antibodies were from Cell Signaling: anti-TSC2, anti-TSC1, anti-p-p70 S6 kinase (T421/424), anti-S6, anti-pS6 (S235/236, D57.2.2E), anti-pS6 (S240/244, D68F8), anti-AKT, anti-pAKT (S473, D9E), anti-pAKT (T308, 244F9), anti-pFOXO1 (S256), anti-FOXO1 (C29H4), and anti–p4E-BP1 (T37/46). Anti-actin and 2DG were purchased from Sigma-Aldrich. BrdU was detected using the BrdU Flow Kit according to the manufacturer's specifications (BD). Other reagents used included OVA Class-I tetramer (H-2 kb/SIINFEKL, Beckman Coulter); IL-2, IL-7, and IL-15 cytokines (all from Pepro Tech); and OVA class-I peptide (SIINFEKL, AnaSpec). Stimulatory anti-CD3 (2C11) and anti-CD28 (37.51) were purified from hybridoma supernatants prepared in-house. Rapamycin was purchased from LC Laboratories. CFSE and MitoTracker Green FM were obtained from Invitrogen. GolgiPlug or GolgiStop (BD Biosciences) was used to inhibit cytokine secretion, and the FOXP3 Fixation/Permeabilization Kit (eBioscience) was used for intracellular staining procedures.

T cell in vitro and ex vivo stimulation. In vitro stimulation of splenocytes was performed with soluble anti-CD3 (1 μg/ml) for 48 hours, followed by a 10-fold media expansion with IL-2 (1 ng/ml) or IL-7 (10 ng/ml) and IL-15 (20 ng/ml) for 3 to 5 days. Live cells were collected by density gradient separation (Ficoll, GE Healthcare) and then restimulated with plate-bound anti-CD3 (1 μg/ml) and soluble anti-CD28 (2 μg/ml) in the presence of GolgiPlug (BD Biosciences) overnight. For ex vivo stimulation, cells were stimulated with 10 μg/ml OVA class I peptide (SIINFEKL) overnight with GolgiPlug. Purified $CD8^+$ T cells were stimulated with plate-bound anti-CD3 (1 μg/ml) and soluble anti-CD28 (2 μg/ml).

Flow cytometry and cell sorting. All experiments were performed on a BD FACSCalibur or LSR II and analyzed using FlowJo software analysis. Naive cells were obtained after sorting for the $CD8^+CD62L^{hi}CD44^{lo}$ population on a BD FACSAria II. For all flow cytometry experiments, gates were set appropriately with unstimulated and isotype controls.

Immunoblot analysis. Magnetically purified $CD8^+$ T cells (MACS, Miltenyi Biotech) were stimulated with 1 μg/ml anti-CD3, 2 μg/ml anti-CD28, and 0.75 μg/ml anti-hamster IgG1 (BD Biosciences). Samples were flash frozen at each time point and lysed in whole-cell lysis buffer with NaF, PI, PMSF, and NaOV3. Proteins were detected by ECL Plus substrate (GE Healthcare). All images were captured using the UVP Biospectrum500 Imaging System.

Vaccinia infection and Listeria rechallenge. WT, T-*Tsc2*$^{-/-}$, and T-*Rheb*$^{-/-}$ mice were infected with 1×10^6 PFU vaccinia-OVA (made in house) by i.p. injection. Six or thirty days after challenge, splenocytes were harvested. For adoptive transfer experiments, C57BL/6 $CD90.2^+$ host mice (The Jackson Laboratory) were infected with 1×10^6 PFU vaccinia-OVA i.p. and were given 1×10^6 (unless otherwise noted) $CD8^+CD90.1^+$ OT-I^+ T cells by retro-orbital (r.o.) injection from WT, T-*Tsc2*$^{-/-}$, T-*Rheb*$^{-/-}$, or T-*Rictor*$^{-/-}$ OT-I^+ mice. Recovery of adoptively transferred OT-I^+ cells was based on $CD8^+CD90.1^+$ staining. A cohort of mice received daily administration of 100 μg/kg rapamycin i.p. from day 5 to 21. Some mice received a secondary infection with 2×10^6 colony-forming units of lm-OVA i.p. (Lm-626-YNG; gift from Charles Drake, Johns Hopkins University School of Medicine) on day 21. Mice were sacrificed 6 days after infection, and splenocytes were isolated for analysis. For naive adoptive transfer experiments, cells

were sorted based on a $CD8^+V\beta5.1^+/V\beta5.2^+CD90.1^+CD44^{lo}CD62L^{hi}$ gating strategy. 1×10^5 cells were injected r.o. into recipients infected with 1×10^6 PFU vaccinia-OVA i.p. For the secondary adoptive transfer experiment, splenocytes were harvested 35 days after naive adoptive transfer and infection. Cells were sorted for the $CD8^+CD90.1^+$ population. 7.5×10^4 sorted cells were injected r.o. into naive WT $CD90.2^+$ recipients infected with 1×10^6 PFU vaccinia-OVA i.p. The percentage of recovered $CD8^+CD90.1^+$ T cells was determined 6 days after transfer. For in vivo 2DG treatment, mice received daily doses of 500 mg/kg 2DG i.p.

In vivo CTL assay. Target cells obtained from WT C57/B6 splenocytes were split into 2 conditions. Half of the cells were labeled with 5 μM CFSE and pulsed with 3 μg/ml OVA-I peptide. The remaining cells were labeled with 0.5 μM CFSE and not peptide pulsed. Cells from both conditions were mixed at a 1:1 ratio, and 8×10^6 cells were injected i.v. into mice that had been infected with vaccinia-OVA 6 days prior. Ten hours after injection, spleens were harvested and CFSE-labeled populations were detected by flow cytometry. The percentage lysis was calculated after taking into account the proportion of CFSE populations found in naive WT mice, using the following calculation: $100 \times (1 - [\%\ \text{experimental CFSE}^{hi}/\%\ \text{experimental CFSE}^{lo}]/[\%\ \text{naive CFSE}^{hi}/\%\ \text{naive CFSE}^{lo}])$.

Tumor experiments. For the thymoma model, 1×10^6 EL4 cells expressing luciferase (EL4-LUCI; gift of Hyam Levitsky, Johns Hopkins University School of Medicine) were injected s.q. into WT or T-*Tsc2*$^{-/-}$ mice. After administration, tumor burden was assessed by measuring luminescence on a Xenogen IVIS 10 minutes after i.p. injection of 1.5 mg/kg D-luciferin firefly salt (Caliper LifeSciences). For the nonluciferase EL4-OVA line, 1×10^6 EL4-OVA cells were injected s.q. into WT, T-*Rheb*$^{-/-}$, T-*Tsc2*$^{-/-}$, T-*Rictor*$^{-/-}$, or littermate control mice. For the B16 melanoma model, C57BL/6 WT mice received a s.q. injection of 2×10^5 B16-OVA melanoma cells (gift of Hyam Levitsky) cultured in vitro under OVA selection media containing 400 μg/ml G418 (Life technologies). Six days after tumor injection, mice received an adoptive transfer of 1.5×10^6 activated T-*Rheb*$^{-/-}$, T-*Tsc2*$^{-/-}$, *Rheb*$^{fl/fl}$, or *Tsc2*$^{fl/fl}$ OT-I$^+$ cells derived from splenocytes, which had been stimulated in vitro with SIINFEKL peptide for 48 hours, sorted for $CD8^+CD90.1^+CD44^+$ population, and expanded in IL-2 for 24 hours. For nonluciferase tumors, tumor burden was assessed every 2 to 4 days by measuring length and width of tumor. Tumor volume was calculated using the formula for the prolate ellipsoid, $(L \times W^2)/2$, where L represents length and is the longer of the 2 measurements and W represents width.

Real-time PCR. Cells were stimulated for 48 hours and then expanded in media supplemented with IL-7 (10 ng/ml) and IL-15 (20 ng/ml) for 3 days. Total RNA was collected using TRIzol reagent (Life Technologies). cDNA was generated with the M-MuLV RT Kit (New England BioLabs), and real-time PCR was performed using TaqMan Universal Master Mix II (Invitrogen). Real-time PCR primers and probes were obtained from Applied Biosystems: *Pfkl* (Mm00435587_m1), *Slc2a1* (Glut1, Mm00441480_m1), *Cpt1a* (Mm01231183_m1), and *Bcl211* (BCL-XL Mm00437783_m1). $\Delta\Delta C_t$ values were normalized to levels of housekeeping gene *18S* ribosomal RNA (Life Technologies). Relative expression is shown in comparison to WT levels (unless otherwise noted). Analysis was performed on an ABI OneStepPlus 96-well instrument.

Metabolic assays. Experiments were performed using the Extracellular Flux Assay Kit (ECAR and OCR) and run on XF 96 Extracellular Flux Analyzer (Seahorse Biosciences). Preparation of cells was as described above in *Real-time PCR*. 1.5×10^5 cells were plated per well on poly-D-lysine–coated TC-treated XF96 cell culture microplates. Plating Seahorse media contained 25 mM glucose, 2 mM L-glutamine, and 1 mM Na pyruvate in XF Assay Medium Modified DMEM (Seahorse Biosciences). Mitochondrial inhibitors used were Oligomycin (an inhibitor of mitochondrial ATP synthase, final concentration 2 μM) and FCCP (an oxidative phosphorylation uncoupler, final concentration 0.5 mM), both from Sigma-Aldrich. SRC was determined by dividing the OCR after FCCP administration by the OCR before addition of inhibitors. For immediate assessment of ECAR and OCR upon restimulation, isolated $CD8^+$ T cells were stimulated with plate-bound αCD3 and soluble αCD28 for 48 hours and then expanded into media supplemented with IL-7/IL-15 for 4 days. 2.5×10^5 live cells were loaded per well in a lysine-coated TC-treated XF96 cell culture microplate in Seahorse media. The plate was loaded into an XF 96 Extracellular Flux Analyzer (Seahorse Biosciences) and rested for 60 minutes prior to stimulation with soluble αCD3/αCD28 (1 μg/ml final concentration). ECAR and OCR were determined every 6 minutes for a total of 734 minutes. The FAO assay was also run on the XF 96 Extracellular Flux Analyzer. Cells were cultured in KHB assay medium (111 mM NaCl, 4.7 mM KCl, 2 mM $MgSO_4$, 1.2 mM Na_2HPO_4, 2.5 mM glucose, 0.5 mM carnitine). XF Palmitate-BSA FAO Substrate (PALM-BSA) was obtained from Seahorse bioscience. Etomoxir, an inhibitor of CPT1A, was added at a final concentration of 200 μM. Addition of BSA alone served as a control. PALM-BSA indicates palmitate-conjugated BSA, a substrate for lipid oxidation.

Statistics. All graphs were created using GraphPad Prism software, and statistical analyses were calculated using GraphPad Prism, except for repeated-measures analyses, which were calculated through an R statistical program. Comparisons between 2 independent groups were assessed by Mann-Whitney *t* tests; comparisons among 3 or more independent groups were calculated by a Kruskal-Wallis ANOVA with a Dunn's post-test. A P value of less than 0.05 was considered statistically significant. Statistical analysis of multiple comparison survival curves was determined after performing Mantel-Cox tests comparing each parameter and correcting the significant P value based upon the Bonferroni correction. Repeated-measures analysis was assessed using R software, where group, time, and interaction between group and time were assayed for significance. All results were confirmed by at least 3 independent experiments. Error bars represent mean ± SEM.

Study approval. All mouse procedures were approved by the Johns Hopkins University Institutional Animal Care and Use Committee and were compliant with the *Guide for the Care and Use of Laboratory Animals* (8th ed. The National Academies Press. 2011.).

Acknowledgments

We thank Drew Pardoll and members of the Powell lab for reviewing the manuscript. We thank Ada Tam and Lee Blosser for assistance with flow cytometry sorting and Brian Herb and Christopher Gamper for assistance with statistical analysis. This work was supported by NIH grants AI072677, AI77610, and AI091481.

Address correspondence to: Jonathan Powell, 1650 Orleans St., CRB-1 Rm 443, Baltimore, Maryland 21287, USA. Phone: 410.502.7887; E-mail: poweljo@jhmi.edu.

1. Kaech SM, Cui W. Transcriptional control of effector and memory CD8+ T cell differentiation. *Nat Rev Immunol*. 2012;12(11):749–761.
2. Williams MA, Bevan MJ. Effector and memory CTL differentiation. *Annu Rev Immunol*. 2007;25:171–192.
3. Frauwirth KA, et al. The CD28 signaling pathway regulates glucose metabolism. *Immunity*. 2002;16(6):769–777.
4. Jones RG, Thompson CB. Revving the engine: signal transduction fuels T cell activation. *Immunity*. 2007;27(2):173–178.
5. Gerriets VA, Rathmell JC. Metabolic pathways in T cell fate and function. *Trends Immunol*. 2012;33(4):168–173.
6. van der Windt GJ, et al. Mitochondrial respiratory capacity is a critical regulator of CD8+ T cell memory development. *Immunity*. 2012;36(1):68–78.
7. Pollizzi KN, Powell JD. Integrating canonical and metabolic signalling programmes in the regulation of T cell responses. Nature reviews. *Immunology*. 2014;14(7):435–446.
8. Zoncu R, Efeyan A, Sabatini DM. mTOR: from growth signal integration to cancer, diabetes and ageing. *Nat Rev Mol Cell Biol*. 2011;12(1):21–35.
9. Dibble CC, et al. TBC1D7 is a third subunit of the TSC1-TSC2 complex upstream of mTORC1. *Mol Cell*. 2012;47(4):535–546.
10. Inoki K, Li Y, Xu T, Guan KL. Rheb GTPase is a direct target of TSC2 GAP activity and regulates mTOR signaling. *Genes Dev*. 2003;17(15):1829–1834.
11. Tee AR, Fingar DC, Manning BD, Kwiatkowski DJ, Cantley LC, Blenis J. Tuberous sclerosis complex-1 and -2 gene products function together to inhibit mammalian target of rapamycin (mTOR)-mediated downstream signaling. *Proc Natl Acad Sci U S A*. 2002;99(21):13571–13576.
12. Laplante M, Sabatini DM. mTOR signaling in growth control and disease. *Cell*. 2012;149(2):274–293.
13. O'Brien TF, et al. Regulation of T-cell survival and mitochondrial homeostasis by TSC1. *Eur J Immunol*. 2011;41(11):3361–3370.
14. Yang K, Neale G, Green DR, He W, Chi H. The tumor suppressor Tsc1 enforces quiescence of naive T cells to promote immune homeostasis and function. *Nat Immunol*. 2011;12(9):888–897.
15. Wu Q, et al. The tuberous sclerosis complex -mammalian target of rapamycin pathway maintains the quiescence and survival of naive T cells. *J Immunol*. 2011;187(3):1106–1112.
16. Zhang L, et al. TSC1/2 signaling complex is essential for peripheral naive CD8+ T cell survival and homeostasis in mice. *PLoS One*. 2012;7(2):e30592.
17. Delgoffe GM, et al. The kinase mTOR regulates the differentiation of helper T cells through the selective activation of signaling by mTORC1 and mTORC2. *Nat Immunol*. 2011;12(4):295–303.
18. Lee K, et al. Mammalian target of rapamycin protein complex 2 regulates differentiation of Th1 and Th2 cell subsets via distinct signaling pathways. *Immunity*. 2010;32(6):743–753.
19. Delgoffe GM, et al. The mTOR kinase differentially regulates effector and regulatory T cell lineage commitment. *Immunity*. 2009;30(6):832–844.
20. Tee AR, Manning BD, Roux PP, Cantley LC, Blenis J. Tuberous sclerosis complex gene products, Tuberin and Hamartin, control mTOR signaling by acting as a GTPase-activating protein complex toward Rheb. *Curr Biol*. 2003;13(15):1259–1268.
21. Hernandez O, Way S, McKenna J 3rd, Gambello MJ. Generation of a conditional disruption of the Tsc2 gene. *Genesis*. 2007;45(2):101–106.
22. Chong-Kopera H, et al. TSC1 stabilizes TSC2 by inhibiting the interaction between TSC2 and the HERC1 ubiquitin ligase. *J Biol Chem*. 2006;281(13):8313–8316.
23. Yee WM, Worley PF. Rheb interacts with Raf-1 kinase and may function to integrate growth factor- and protein kinase A-dependent signals. *Mol Cell Biol*. 1997;17(2):921–933.
24. Kaech SM, Tan JT, Wherry EJ, Konieczny BT, Surh CD, Ahmed R. Selective expression of the interleukin 7 receptor identifies effector CD8 T cells that give rise to long-lived memory cells. *Nat Immunol*. 2003;4(12):1191–1198.
25. Joshi NS, et al. Inflammation directs memory precursor and short-lived effector CD8(+) T cell fates via the graded expression of T-bet transcription factor. *Immunity*. 2007;27(2):281–295.
26. Intlekofer AM, et al. Effector and memory CD8+ T cell fate coupled by T-bet and eomesodermin. *Nat Immunol*. 2005;6(12):1236–1244.
27. Araki K, et al. mTOR regulates memory CD8 T-cell differentiation. *Nature*. 2009;460(7251):108–112.
28. Rao RR, Li Q, Odunsi K, Shrikant PA. The mTOR kinase determines effector versus memory CD8+ T cell fate by regulating the expression of transcription factors T-bet and Eomesodermin. *Immunity*. 2010;32(1):67–78.
29. Banerjee A, et al. Cutting edge: The transcription factor eomesodermin enables CD8+ T cells to compete for the memory cell niche. *J Immunol*. 2010;185(9):4988–4992.
30. Deberardinis RJ, Lum JJ, Thompson CB. Phosphatidylinositol 3-kinase-dependent modulation of carnitine palmitoyltransferase 1A expression regulates lipid metabolism during hematopoietic cell growth. *J Biol Chem*. 2006;281(49):37372–37380.
31. Zaugg K, et al. Carnitine palmitoyltransferase 1C promotes cell survival and tumor growth under conditions of metabolic stress. *Genes Dev*. 2011;25(10):1041–1051.
32. Cham CM, Driessens G, O'Keefe JP, Gajewski TF. Glucose deprivation inhibits multiple key gene expression events and effector functions in CD8+ T cells. *Eur J Immunol*. 2008;38(9):2438–2450.
33. Sarbassov DD, Guertin DA, Ali SM, Sabatini DM. Phosphorylation and regulation of Akt/PKB by the rictor-mTOR complex. *Science*. 2005;307(5712):1098–1101.
34. Kerdiles YM, et al. Foxo1 links homing and survival of naive T cells by regulating L-selectin, CCR7 and interleukin 7 receptor. *Nat Immunol*. 2009;10(2):176–184.
35. Fabre S, et al. Stable activation of phosphatidylinositol 3-kinase in the T cell immunological synapse stimulates Akt signaling to FoxO1 nuclear exclusion and cell growth control. *J Immunol*. 2005;174(7):4161–4171.
36. Cornish GH, Sinclair LV, Cantrell DA. Differential regulation of T-cell growth by IL-2 and IL-15. *Blood*. 2006;108(2):600–608.
37. Krishna S, Yang J, Wang H, Qiu Y, Zhong XP. Role of tumor suppressor TSC1 in regulating antigen-specific primary and memory CD8 T cell responses to bacterial infection. *Infect Immun*. 2014;82(7):3045–3057.
38. Cham CM, Gajewski TF. Glucose availability regulates IFN-gamma production and p70S6 kinase activation in CD8+ effector T cells. *J Immunol*. 2005;174(8):4670–4677.
39. van der Windt GJ, Pearce EL. Metabolic switching and fuel choice during T-cell differentiation and memory development. *Immunol Rev*. 2012;249(1):27–42.
40. Powell JD, Pollizzi KN, Heikamp EB, Horton MR. Regulation of immune responses by mTOR. *Annu Rev Immunol*. 2012;30:39–68.
41. Shrestha S, Yang K, Wei J, Karmaus PW, Neale G, Chi H. Tsc1 promotes the differentiation of memory CD8+ T cells via orchestrating the transcriptional and metabolic programs. *Proc Natl Acad Sci U S A*. 2014;111(41):14858–14863.
42. Zhu L, et al. TSC1 controls macrophage polarization to prevent inflammatory disease. *Nat Commun*. 2014;5:4696.
43. Goncharova EA, James ML, Kudryashova TV, Goncharov DA, Krymskaya VP. Tumor suppressors TSC1 and TSC2 differentially modulate actin cytoskeleton and motility of mouse embryonic fibroblasts. *PLoS One*. 2014;9(10):e111476.
44. Rosner M, Hanneder M, Siegel N, Valli A, Hengstschlager M. The tuberous sclerosis gene products hamartin and tuberin are multifunctional proteins with a wide spectrum of interacting partners. *Mutat Res*. 2008;658(3):234–246.
45. Sancak O, et al. Mutational analysis of the TSC1 and TSC2 genes in a diagnostic setting: genotype — phenotype correlations and comparison of diagnostic DNA techniques in Tuberous Sclerosis Complex. *Eur J Hum Genet*. 2005;13(6):731–741.
46. Duvel K, et al. Activation of a metabolic gene regulatory network downstream of mTOR complex 1. *Mol Cell*. 2010;39(2):171–183.
47. Yang K, et al. T cell exit from quiescence and differentiation into Th2 cells depend on Raptor-mTORC1-mediated metabolic reprogramming. *Immunity*. 2013;39(6):1043–1056.
48. van der Windt GJ, et al. CD8 memory T cells have a bioenergetic advantage that underlies their rapid recall ability. *Proc Natl Acad Sci U S A*. 2013;110(35):14336–14341.
49. Turner AP, et al. Sirolimus enhances the magnitude and quality of viral-specific CD8+ T-cell responses to vaccinia virus vaccination in rhesus macaques. *Am J Transplant*. 2011;11(3):613–618.
50. Chen CH, et al. ER stress inhibits mTORC2 and Akt signaling through GSK-3β-mediated phosphorylation of rictor. *Sci Signal*. 2011;4(161):ra10.
51. Li Q, et al. Regulating mammalian target of rapamycin to tune vaccination-induced CD8(+) T cell responses for tumor immunity. *J Immunol*. 2012;188(7):3080–3087.
52. Sukumar M, et al. Inhibiting glycolytic metabolism enhances CD8+ T cell memory and antitumor function. *J Clin Invest*. 2013;123(10):4479–4488.
53. Berezhnoy A, Castro I, Levay A, Malek TR, Gilboa E. Aptamer-targeted inhibition of mTOR in T

cells enhances antitumor immunity. *J Clin Invest*. 2014;124(1):188–197.
54. Schluns KS, Williams K, Ma A, Zheng XX, Lefrancois L. Cutting edge: requirement for IL-15 in the generation of primary and memory antigen-specific CD8 T cells. *J Immunol*. 2002;168(10):4827–4831.
55. Sebzda E, Zou Z, Lee JS, Wang T, Kahn ML. Transcription factor KLF2 regulates the migration of naive T cells by restricting chemokine receptor expression patterns. *Nat Immunol*. 2008;9(3):292–300.
56. Sinclair LV, et al. Phosphatidylinositol-3-OH kinase and nutrient-sensing mTOR pathways control T lymphocyte trafficking. *Nat Immunol*. 2008;9(5):513–521.
57. Hess Michelini R, Doedens AL, Goldrath AW, Hedrick SM. Differentiation of CD8 memory T cells depends on Foxo1. *J Exp Med*. 2013;210(6):1189–1200.
58. Tejera MM, Kim EH, Sullivan JA, Plisch EH, Suresh M. FoxO1 controls effector-to-memory transition and maintenance of functional CD8 T cell memory. *J Immunol*. 2013;191(1):187–199.
59. Gubser PM, et al. Rapid effector function of memory $CD8^+$ T cells requires an immediate-early glycolytic switch. *Nat Immunol*. 2013;14(10):1064–1072.
60. Crompton JG, et al. Akt inhibition enhances expansion of potent tumor-specific lymphocytes with memory cell characteristics. *Cancer Res*. 2015;75(2):296–305.
61. Araki K, Youngblood B, Ahmed R. The role of mTOR in memory CD8 T-cell differentiation. *Immunol Rev*. 2010;235(1):234–243.
62. Kumar A, et al. Muscle-specific deletion of rictor impairs insulin-stimulated glucose transport and enhances Basal glycogen synthase activity. *Mol Cell Biol*. 2008;28(1):61–70.